Taylor & Francis
Taylor & Francis Group

Australian Journal of Earth Sciences

An International Geoscience Journal of the Geological Society of Australia

ISSN: 0812-0099 (Print) 1440-0952 (Online) Journal homepage: www.tandfonline.com/journals/taje20

# Tectonic switching within a long-lived convergent margin: evidence from the geochemistry of Paleoproterozoic granitoids, Dajarra region, Mount Isa Inlier

S. Noptalung, I. V. Sanislav, H. A. Cocker, A. A. Kumar & M. Sami

**To cite this article:** S. Noptalung, I. V. Sanislav, H. A. Cocker, A. A. Kumar & M. Sami (22 Apr 2026): Tectonic switching within a long-lived convergent margin: evidence from the geochemistry of Paleoproterozoic granitoids, Dajarra region, Mount Isa Inlier, Australian Journal of Earth Sciences, DOI: 10.1080/08120099.2026.2655335

**To link to this article:** https://doi.org/10.1080/08120099.2026.2655335

AUSTRALIAN JOURNAL OF EARTH SCIENCES
https://doi.org/10.1080/08120099.2026.2655335



# Tectonic switching within a long-lived convergent margin: evidence from the geochemistry of Paleoproterozoic granitoids, Dajarra region, Mount Isa Inlier

S. Noptalung[a,b], I. V. Sanislav[a,b], H. A. Cocker[a,b], A. A. Kumar[a,b] and M. Sami[c]

[a]Economic Geology Research Centre (EGRU), James Cook University, Townsville, QLD, Australia; [b]Earth and Environmental Science, College of Science and Engineering, James Cook University, Townsville, QLD, Australia; [c]Geosciences Department, College of Science, United Arab Emirates University, Al Ain, United Arab Emirates

**ABSTRACT**

Paleoproterozoic granitoids of the Mount Isa Inlier record a prolonged history of crustal magmatism linked to the tectonic evolution of the North Australian Craton during assembly of the Nuna supercontinent. This study presents a lithogeochemical investigation of intrusions from the Dajarra region, in the southern Western Fold Belt, to constrain their geochemical characteristics, petrogenesis, and tectonic setting. The intrusions were emplaced at *ca* 1850–1650 Ma and correspond to four major magmatic episodes: the Kalkadoon, Argylla, Wonga-Burstall and Sybella igneous events. Thirty-three representative samples of plutons and associated dykes were analysed for whole-rock major and trace elements. The granitoids are dominantly felsic ($SiO_2$, 62.6–76.7 wt%), with low MgO and $TiO_2$ contents, high total alkalis and coherent fractionation trends consistent with extreme magmatic differentiation. Most samples are ferroan, alkalic-calcic to calc-alkalic and strongly peraluminous, whereas the Kalkadoon (KIE) sample is metaluminous. Trace-element patterns are characterised by enrichment in large ion lithophile elements and high-field-strength elements (HFSEs), pronounced negative Nb, Ti, Sr and Eu anomalies, and moderately to strongly fractionated rare earth element patterns. Distinct geochemical differences are observed between granitoid suites and across major structural boundaries, notably between Argylla intrusions east (AIE-E) and west (AIE-W) of the Rufus Fault. Many AIE-E, Wonga-Burstall and Sybella samples display elevated HFSE abundances and high zircon saturation temperatures, whereas AIE-W samples are HFSE-poor and exhibit lower temperatures, consistent with S-type affinities. On granite discrimination diagrams, most samples plot near the I- and A-type boundary and mainly within the $A_2$ field, indicating derivation from reworked continental crust. This suggests that granitoid magmatism in the Dajarra region was dominated by partial melting of continental crust, with episodic mantle input required to achieve high melt temperatures. The magmatism occurred within a long-lived convergent margin system characterised by tectonic switching between contractional and extensional regimes during the Paleoproterozoic evolution of the Mount Isa Inlier.

**KEY POINTS**

1. Paleoproterozoic granitoids in the Dajarra region record highly felsic magmatism with extreme magmatic differentiation.
2. Geochemical data indicate that felsic magmas formed mainly by crustal melting, with variable thermal input, in a subduction-related setting.
3. Magmatism was controlled by a long-lived convergent margin characterised by tectonic switching in the Mount Isa Inlier.

**ARTICLE HISTORY**
Received 1 February 2026
Accepted 30 March 2026

**KEYWORDS**
Geochemistry; Paleoproterozoic granitoids; tectonic switching; convergent margin; Mount Isa Inlier; North Australian Craton

## Introduction

Proterozoic granites and their comagmatic volcanic equivalents are widely preserved within the Mount Isa Inlier. Over the past few decades, geochronological studies have been conducted to constrain the timing and duration of magmatic activity within the inlier (*e.g.* Brown *et al.*, 2023; Bultitude *et al.*, 2021; Cocker *et al.*, 2025; Noptalung *et al.*, 2026). Six major magmatic episodes have been defined: the 1880–1850 Ma Kalkadoon Igneous Event, the 1820–1770 Ma Argylla Igneous Event, the 1750–1690 Ma Burstall-Wonga Igneous Event, the 1680–1650 Ma Sybella Igneous Event, the 1640–1610 Ma Tommy Creek Igneous Event and the 1550–1490 Ma William Igneous Event, with exposures distributed across different structural domains of the Mount Isa Inlier (Figure 1). The timing of magmatism broadly coincides with major tectonic events affecting Proterozoic Australian cratons and the assembly of the Nuna supercontinent

**CONTACT** S. Noptalung sutthida.noptalung@my.jcu.edu.au Economic Geology Research Centre (EGRU), James Cook University, Townsville, QLD 4811, Australia

Supplemental data for this article can be accessed online at https://doi.org/10.1080/08120099.2026.2655335.
Editorial handling: Chris Fergusson

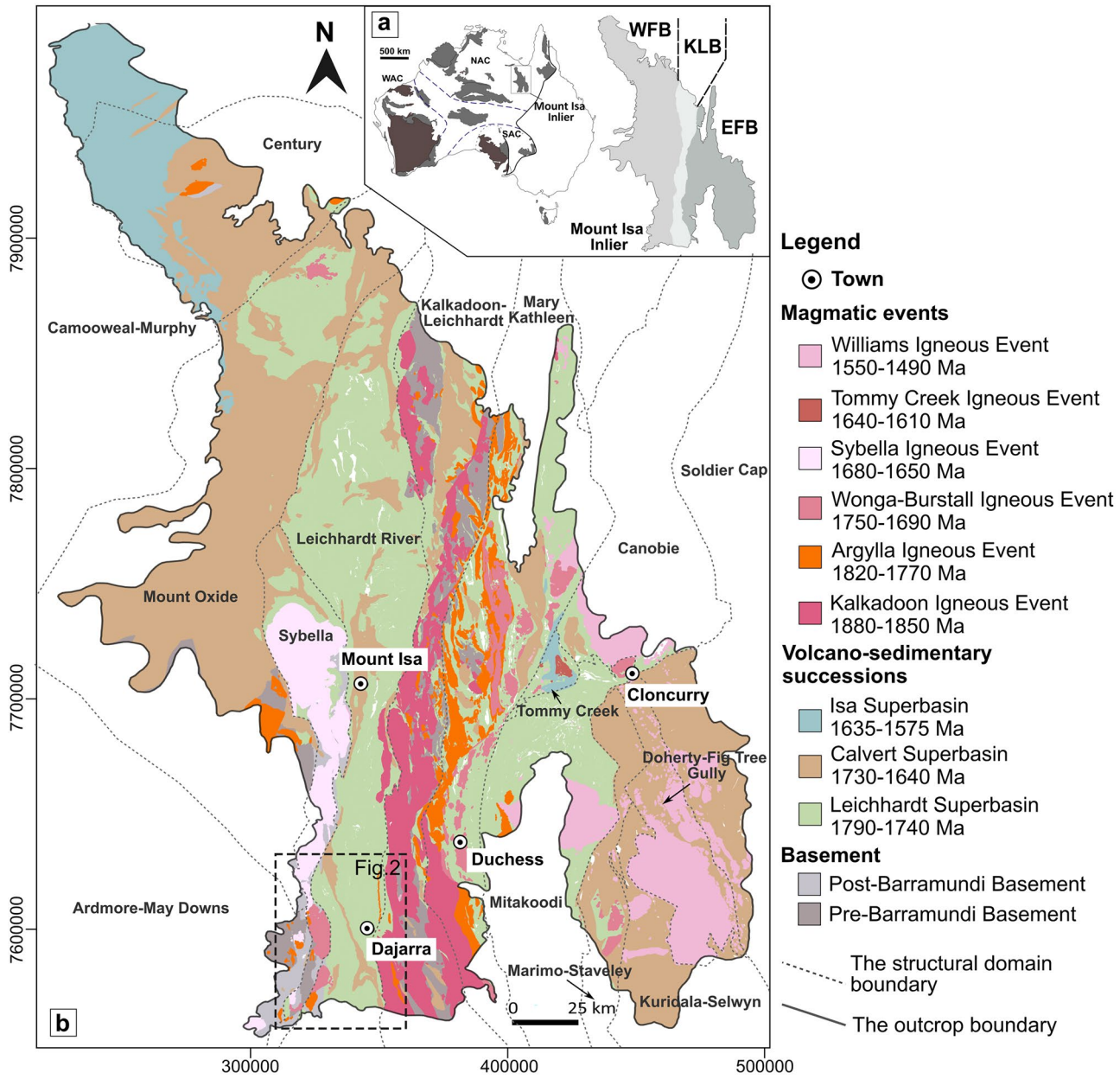


**Figure 1.** (a) Archean–Proterozoic cratons, including the Mount Isa Inlier, which is located within the North Australian Craton (NAC) and subdivided into three tectonostratigraphic components (EFB, Eastern Fold Belt; WFB, Western Fold Belt; KLB, Kalkadoon-Leichhardt Belt). (b) Distribution of stratigraphic units within the Mount Isa Inlier, showing further subdivision into structural domains. The study area, the Dajarra region, is indicated by a dashed box. Coordinates are MGA54.

(*e.g.* Betts & Giles, 2006; Gibson *et al.*, 2020, 2025; Giles *et al.*, 2002; Zhao *et al.*, 2004). However, the petrogenesis of Proterozoic granitoids in the Mount Isa Inlier remains debated, owing to the limited isotopic and geochemical data available to constrain magma sources and evolutionary processes (Wilson, 1978, 1987; Wyborn, 1988; Wyborn *et al.*, 1988, 1992; Wyborn & Page, 1983).

The aim of this study is to characterise the geochemical features, petrogenesis and tectonic setting of granitic intrusions in the Dajarra region, in the southern part of the Western Fold Belt. The emplacement ages of these granites, reported by Noptalung *et al.* (2026), range from *ca* 1850 to 1650 Ma. The lithogeochemical analyses of selected samples include whole-rock major and trace elements, as well as halogen concentrations, with particular emphasis on fluorine. The Dajarra granitoids display geochemical characteristics comparable with those of coeval granites elsewhere in the Mount Isa Inlier. These whole-rock compositions constrain magma sources and associated tectonic settings, indicating that the granitic magmas were generated by partial melting of continental crust, with episodic contributions from juvenile mantle sources. These features suggest that magmatic evolution in the Mount Isa Inlier occurred within a long-lived subduction-related tectonic regime.

## Regional geological setting

The Mount Isa Inlier, located in the eastern region of the North Australian Craton (NAC), comprises three main tectonostratigraphic components: the Eastern Fold Belt (EFB), the Western

Fold Belt (WFB) and the Kalkadoon-Leichhardt Belt (KLB) (Figure 1a). These belts are further subdivided into north–south-trending domains defined by variations in geological settings and the presence of bounding structures (Withnall & Hutton, 2013). These domains preserve magmatic and sedimentary rocks (Figure 1b) recording the geological evolution of the inlier during late Paleoproterozoic to early Mesoproterozoic (*ca* 1880 to 1490 Ma) (Betts *et al.*, 2006; Blake, 1986; Blake & Stewart, 1992; MacCready *et al.*, 1998; Scott *et al.*, 2000).

The first voluminous magmatism, the Kalkadoon Igneous Event (KIE) occurred between *ca* 1880 and 1850 Ma and is predominantly preserved within the KLB (Bierlein *et al.*, 2011; Page, 1983; Wyborn, 1988). The KIE is broadly synchronous with the Barramundi Orogeny, which is a major orogenic event recorded across the NAC (Etheridge *et al.*, 1987; Page & Williams, 1988). Based on the relative relationship to the KIE rocks, two basement units have been distinguished: the Pre-Barramundi and Post-Barramundi basement rocks that predominantly crop out in the WFB. The Pre-Barramundi Basement comprises metasedimentary rocks deposited before *ca* 1870 Ma, which subsequently underwent deformation and metamorphism during the Barramundi Orogeny (Bierlein *et al.*, 2008; Blake & Stewart, 1992). In contrast, the formation and evolution of the Post-Barramundi basement are less understood, and its development appears to terminate with the initiation of magmatism at *ca* 1820 Ma (Carson *et al.*, 2009; Magee *et al.*, 2012; Noptalung *et al.*, 2026; Withnall & Hutton, 2013).

The basement units are overlain by extensive metasedimentary and metavolcanic sequences preserved throughout the Mount Isa Inlier. They are subdivided into three distinctive superbasins (Gibson *et al.*, 2016): the Leichhardt Superbasin (*ca* 1790–1740 Ma), the Calvert Superbasin (*ca* 1730–1640 Ma) and the Isa Superbasin (*ca* 1635–1575 Ma). The Leichhardt Superbasin sequences have been deformed between *ca* 1750 and 1710 Ma by the Wonga Orogeny (Spence *et al.*, 2021, 2022), whereas the Calvert and Isa superbasin sequences have been deformed by the Isan Orogeny between *ca* 1650 and 1490 Ma (Abu Sharib & Sanislav, 2013; Connors & Page, 1995; Gibson *et al.*, 2016; O'Dea *et al.*, 1997b). Recent studies link deformation in the Tick Hill region to compressional events between *ca* 1810 Ma and 1780 Ma (Le *et al.*, 2021b, 2024).

## Tectonic setting

During the Nuna assembly, most of the Australian Proterozoic cratons are interpreted to have experienced an active continental margin tectonic environment that underwent prolonged reworking from *ca* 1880 Ma before the final collision with Laurentia at *ca* 1600 Ma (Betts & Giles, 2006; Gibson *et al.*, 2020, 2025; Noptalung *et al.*, 2026).

The earliest recognised major tectonic event is the Barramundi Orogeny, a regional compressional event between *ca* 1890 and 1850 Ma that affected the entire NAC (Etheridge *et al.*, 1987; Page & Williams, 1988). In the Mount Isa Inlier, the Barramundi Orogeny caused deformation and metamorphism of the Pre-Barramundi basement rocks and was accompanied by magmatism associated with the KIE (Figure 1b). The KIE preserved in the KLB forms part of a magmatic belt that extends into the South Australian Craton (SAC), where it is represented by the coeval intrusion of the Donington Suite. The alignment and distribution of this belt were interpreted to reflect an Andean style subduction system (*e.g.* Bierlein *et al.*, 2011; Gibson *et al.*, 2025; Noptalung *et al.*, 2026; Wyborn *et al.*, 1992). In the Dajarra region, the KIE rocks are found mainly in the eastern part where large plutons crop out, whereas in the western part, only minor intrusive bodies occur within the Sulieman Gneiss (Figure 2).

Following the Barramundi Orogeny, a series of orogenic events occurred along the southern margin of the NAC and produced widespread magmatism in the Arunta Inlier, Granite-Tanami region, and the Halls Creek Orogen between *ca* 1820 and 1770 Ma (Bagas *et al.*, 2010; Claoué-Long, Edgoose, & Worden, 2008; Claoué-Long & Edgoose, 2008; Hand & Buick, 2001; Iaccheri, 2019; Page *et al.*, 2001). This magmatism is broadly synchronous with the Argylla Igneous Event (AIE) in the Mount Isa Inlier (Figure 1b). The granitoid intrusions in the Arunta, Granite-Tanami, and Halls Creek regions were interpreted to represent orogenic processes and collisional tectonics linked to the assembly of the Nuna Supercontinent (Gibson *et al.*, 2025). However, the tectonic setting responsible for contemporaneous magmatism in the Mount Isa Inlier is uncertain. The AIE was originally interpreted to have initiated during intracontinental rifting associated with the opening of the Leichhardt Superbasin, as evidenced by coeval bimodal volcanism throughout the inlier (Derrick, 1982; O'Dea *et al.*, 1997a, 1997b; Page, 1983; Passchier & Williams, 1989). Bimodal volcanic rocks form a north–south-trending volcanic belt along the length of the inlier, which has been interpreted to reflect east–west rifting on either side of the KLB, driven either by mantle plume activity (O'Dea *et al.*, 1997b) or by back-arc extension distal to a magmatic arc in the Arunta Inlier (Giles *et al.*, 2002). Recent studies, however, highlighted extensive plutonism during *ca* 1820–1780 Ma in the Mount Isa Inlier (Cocker *et al.*, 2025; Le *et al.*, 2021a; Noptalung *et al.*, 2026). Noptalung *et al.* (2026) suggested that pluton emplacement between *ca* 1810 and 1770 Ma occurred in a back-arc setting related to subduction along the southern margin of the NAC that is consistent with Hf isotopic compositions indicating mixed sources of reworked older crust and juvenile mantle. In the Tick Hill region, these granitoids exhibit a syn-tectonic upright fabrics correlated with compressional deformation, suggesting that magmatism was at least partially coeval with regional compressional tectonics (Le *et al.*, 2021b, 2024). In the Dajarra region, igneous rocks belonging to the AIE are widespread and occur as plutons and dykes (Figure 2).

The next major tectonic event affecting the NAC occurred between *ca* 1750 and 1690 Ma with well-documented magmatism in the Arunta Inlier (*e.g.* Zhao & Bennett, 1995) and Mount Isa Inlier (*e.g.* Bultitude *et al.*, 2021; Cocker *et al.*, 2025; Withnall, 2019). In the Arunta Inlier, this magmatism was synchronous with the Strangways Orogeny (Claoué-Long *et al.*, 2008; Collins & Shaw, 1995) whereas in the Mount Isa Inlier it occurred synchronously with the Wonga Orogeny (Spence *et al.*, 2021, 2022).

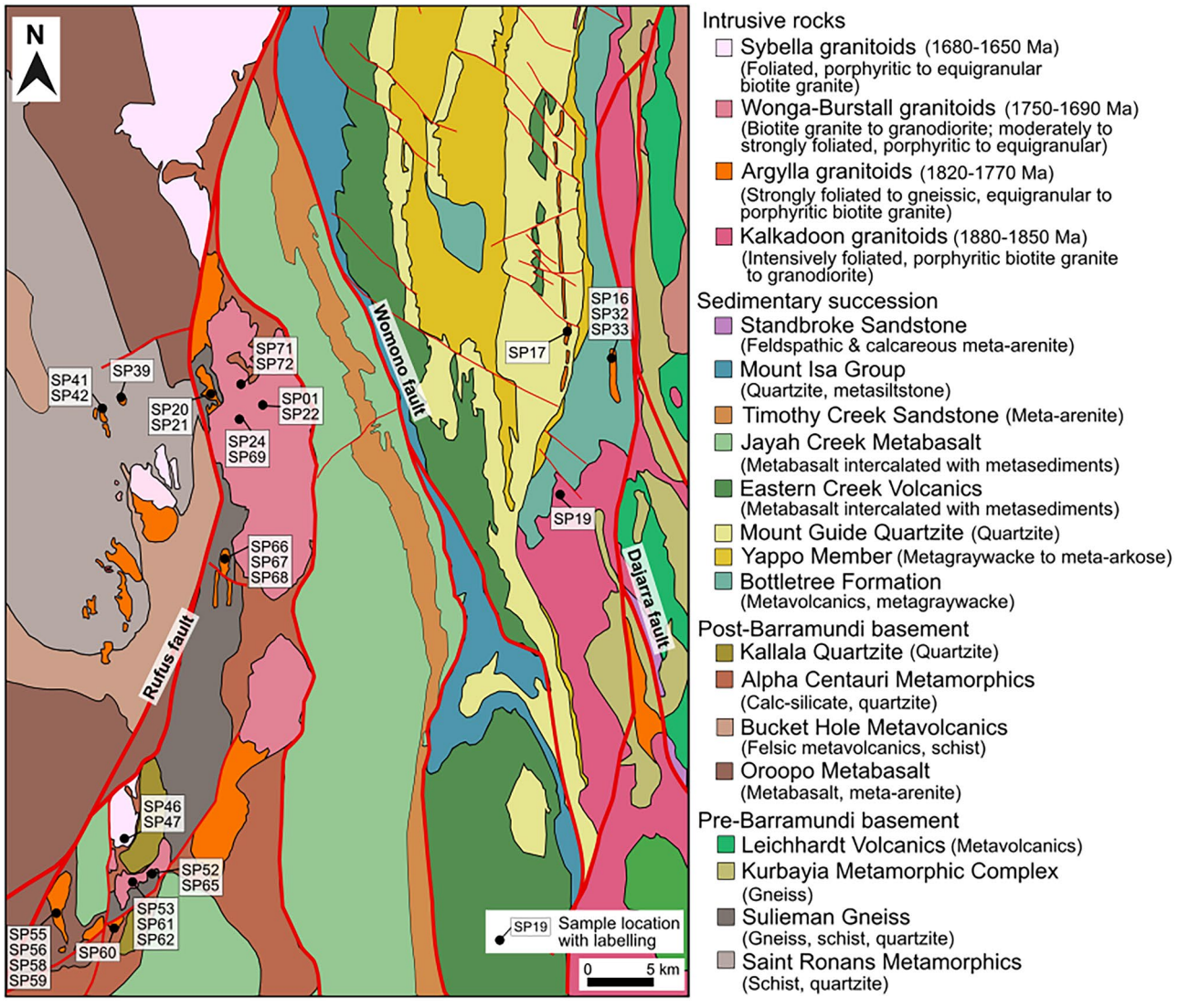


**Figure 2.** Geological map of the Dajarra region showing the distribution of the Kalkadoon, Argylla, Wonga-Burstall, and Sybella granitoid suites, modified after Noptalung *et al.* (2026). Sample locations for lithogeochemical study are indicated.

Geochemical and Nd isotopic data indicate that the granitoids from the Arunta Inlier have an arc-magmatic affinity, consistent with derivation through remelting of older continental crust (Zhao & McCulloch, 1995). A similar subduction-related setting is recorded in the SAC, where *ca* 1750–1690 Ma magmatism corresponds to the Kimban Orogeny (Dutch *et al.*, 2008; Reid *et al.*, 2008; Reid & Hand, 2012). The *ca* 1750–1690 Ma intrusions of the Wonga-Burstall Igneous Event (WBIE) (Figure 1b) granites emplaced during the Wonga Orogeny could also be related to a subduction system along the eastern margin of the NAC (Korsch *et al.*, 2012; Noptalung *et al.*, 2026; Spence *et al.*, 2021, 2022). In the Dajarra region, plutons and dykes belonging to the WBIE record the final stages of this magmatic event, have ages between *ca* 1710 and 1690 Ma, and are found mainly in the central and southern part of the region (Figure 1).

In the Mount Isa Inlier, a major magmatic event occurred between *ca* 1680 and 1650 Ma, the Sybella Igneous Event (SIE), which is mainly represented in the Sybella domain (Figure 1b). This period is interpreted to correspond mainly to crustal extension and opening of the Calvert Superbasin (*e.g.* Gibson *et al.*, 2008, 2016) probably related to a retreating subduction system along the eastern margin of the NAC (*e.g.* Lambeck *et al.*, 2012; Noptalung *et al.*, 2026). A similar extensional signature is recorded in the SAC, with coeval magmatism and sedimentation during this interval (Hand *et al.*, 2007). In the Dajarra region (Figure 2), intrusive rocks belonging to the SIE are found mainly in the western part as moderate size plutons.

The Riversleigh Event at *ca* 1640 Ma recorded in the WFB marks the end of Calvert Superbasin (Gibson *et al.*, 2016, 2020) sedimentation and possibly the onset of the Isan Orogeny (*e.g.* Abu Sharib & Sanislav, 2013; Wyborn *et al.*, 1988). Synchronously, magmatism between *ca* 1640 and 1610 Ma, the Tommy Creek Igneous Event, was interpreted to represent localised basin development (Figure 1b; Brown *et al.*, 2023) during the formation of the Isa Superbasin (Gibson *et al.*, 2012, 2016). The Isan Orogeny (*ca* 1620–1490 Ma; *e.g.* Abu Sharib & Sanislav, 2013; Wyborn *et al.*, 1988) is the last major tectonic event to affect the Mount Isa Inlier. The *ca* 1550–1490 Ma Williams Igneous Event

is the last major magmatic event in the inlier, and plutons of this age are known only from the EFB (Figure 1b; Withnall, 2019).

## Samples from Dajarra region

The granites from the Dajarra region have been previously assigned to the SIE. However, recent U–Pb zircon geochronology was used to reassign the granites from this region to the Kalkadoon, Argylla, Wonga-Burstall and Sybella igneous events (Noptalung *et al.*, 2026). In this study, we sampled granite intrusions and dykes corresponding to all these intrusive events (the sample list is provided in the Supplemental data; Table A1).

### *Kalkadoon Igneous Event (KIE)*

The largest intrusion in the eastern Dajarra region has an emplacement age of 1856 ± 6 Ma and has been assigned to the KIE (Noptalung *et al.*, 2026). The composition of the intrusion ranges from granodiorite to granite. It is medium- to coarse-grained and consists primarily of quartz, feldspar, biotite and hornblende, with K-feldspar phenocrysts up to 2 cm in size. The main phase of the intrusion is equigranular and foliated, whereas porphyritic phases appear undeformed. One sample was collected from a porphyritic unit cropping out along the western margin of the larger intrusion (SP19; Figure 2).

### *Argylla Igneous Event (AIE)*

Granitoid samples from the Argylla Igneous Event were collected from the intrusions cropping out to the east (AIE-E) and west (AIE-W) of the Rufus Fault.

#### *AIE-E samples*

East of the Rufus Fault, the main AIE granites are the Camel Creek Granite, the Graden Creek Porphyry and a series of unnamed north–south-trending plutons occurring close to the Rufus Fault that intrude the Sulieman Gneiss, Oroopo Metabasalt and Alpha Centauri Metamorphics (Figure 2).

The Camel Creek Granite is medium to strongly deformed and contains a well-developed, subvertical foliation trending north–south (Figure 2). The intrusion is medium-grained, composed primarily of quartz, feldspar, and mica (Figure 3b, c). Three samples were collected from this unit, one sample (SP16) from the core of the pluton and two samples (SP32 and SP33) from its marginal zone. The Garden Creek Porphyry is undeformed and intrudes the units mapped as Mount Guide Quartzite (Figure 2). One sample (SP17) was collected from this dyke; it is porphyritic and consists of a fine-grained matrix of quartz, feldspar and biotite, with potassic feldspar (K-feldspar) phenocrysts up to 2–3 cm in length (Figure 3d).

Samples SP20 and SP21 were collected from a small pluton intruding the Sulieman Gneiss in the northwestern part of Dajarra region (Figure 2). This intrusion is strongly foliated, medium to coarse-grained and compositionally varies between granodiorite and granite. The mineralogy consists mainly of variable proportions of quartz, plagioclase, biotite, hornblende and large K-feldspar phenocrysts (Figure 3e).

A small pluton intruding the Sulieman Gneiss in the central part of the Dajarra region was also sampled (Figure 2). Three samples were collected, including two (SP66 and SP67) from the main intrusive phase and one (SP68) from a crosscutting granitic dyke. The intrusion is intensely deformed and exhibits a well-developed gneissic fabric defined by compositional banding and the preferred alignment of mafic minerals and elongate quartz–feldspar aggregates. Mineralogically, the intrusion is relatively homogeneous and is composed predominantly of quartz, K-feldspar and biotite (Figure 3f).

Five samples were collected from a series of plutons intruding the Oroopo Metabasalt in the southwestern part of the Dajarra region (Figure 2). These intrusions are moderately to strongly deformed and commonly contain elongated mafic enclaves, interpreted to be derived from the Oroopo Metabasalt. The rocks are medium- to coarse-grained and consist mainly of quartz, K-feldspar and biotite. Locally, the intrusions display a porphyritic texture, characterised by large K-feldspar phenocrysts up to 2 cm in length set in a medium- to coarse-grained matrix (Figure 3g). Four samples (SP55, SP56, SP58 and SP60) were collected from the main intrusive phase, while one sample (SP59) was collected from a crosscutting felsic dyke.

#### *AIE-W samples*

Three samples were collected from small granitic bodies cropping out west of the Rufus Fault and intruding the Saint Ronans Metamorphics (Figure 2). These intrusions are weakly deformed, pink to greyish pink in colour, medium-grained and composed mainly of quartz, K-feldspar, plagioclase, biotite and muscovite (Figure 3h–j).

### *Wonga-Burstall Igneous Event (WBIE)*

The WBIE granitoids occur mainly on the eastern side of the Rufus Fault and intrude the Sulieman Gneiss and the Alpha Centauri Metamorphics (Figure 2). They form an approximately north–south-trending belt of various size plutons, small intrusions and dykes. Two plutons were sampled, the Steeles Granite (WBIE-S) that forms a large pluton in the middle of the study area and the Copper Valley Granite (WBIE-CV) that occurs as a series of smaller plutons in the southern part of the study area.

#### *WBIE-S samples*

The Steeles Granite (WBIE-S) is a composite pluton consisting mainly of porphyritic biotite granite to granodiorite and minor amounts of medium-grained granodiorite to diorite. The pluton is variably deformed with porphyritic granite and granodiorite phases being the least deformed, whereas the equigranular granodiorite and diorite phases can be strongly deformed. The porphyritic phase consists mainly of quartz, feldspar, biotite and minor hornblende with large K-feldspar phenocrysts up to 3 cm in length (Figure 3k, l). The medium-grained granodiorite displays a similar mineralogical composition and has a higher

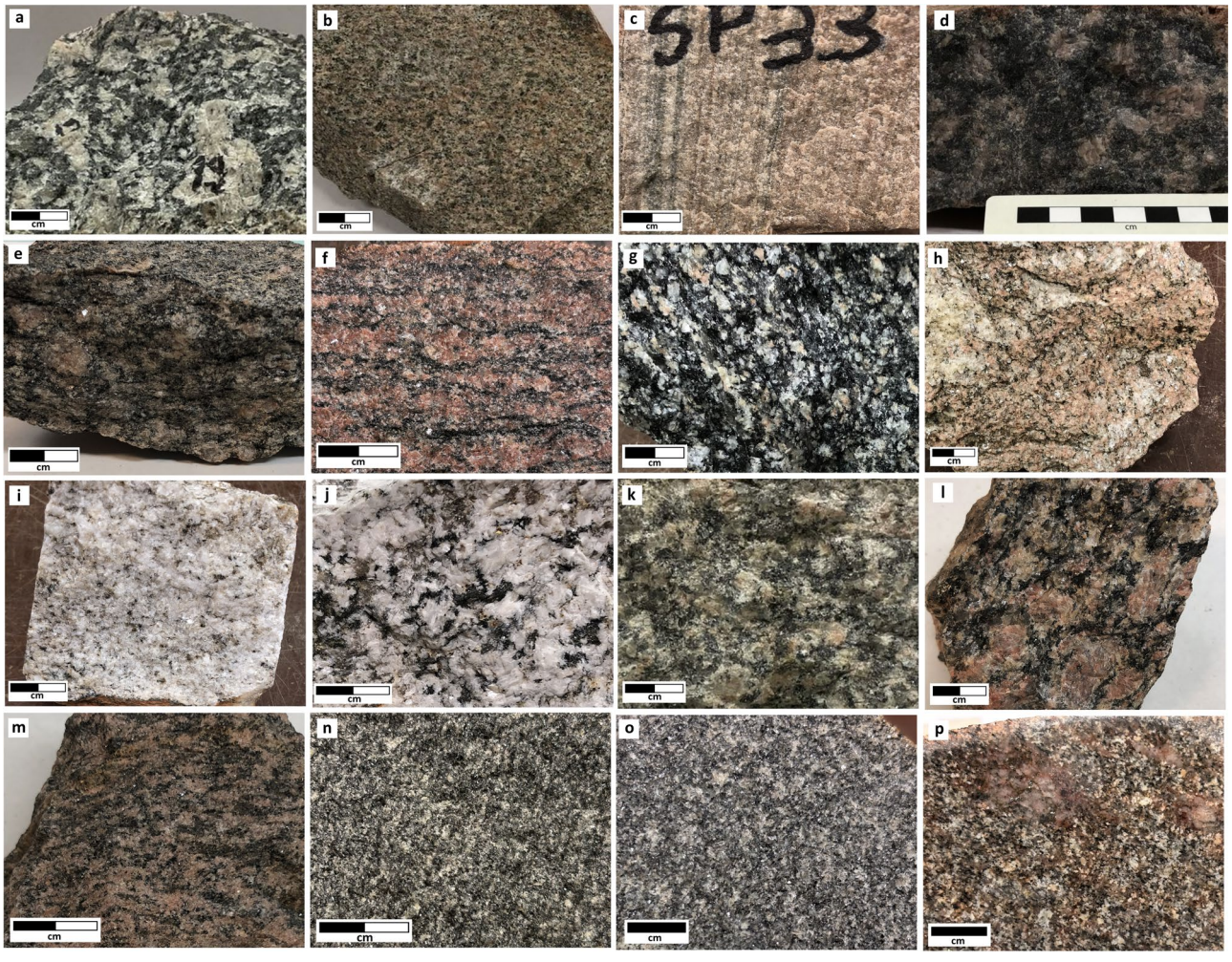


**Figure 3.** Hand-specimen photographs of granitoids in the Dajarra region; Kalkadoon (a), Argylla (b–j), Wonga-Burstall (k–o) and Sybella (p) granitoids. (a) Kalkadoon granite characterised by a coarse-grained texture with large feldspar phenocrysts. (b–c) Camel Creek Granite, showing variable deformation intensity, with the core exhibiting weaker deformation (b) that progressively increases toward the rim (c). (d) Garden Creek Porphyry, a microgranite containing pink K-feldspar phenocrysts. (e) Representative sample of AIE-E (SP20 and SP21) characterised by a strongly foliated granite containing K-feldspar phenocrysts. (f) Representative AIE-E sample (SP66 and SP67), exposed as a granite exhibiting strong foliation grading into a gneissic fabric. (g) Representative AIE-E sample (SP55, SP56 and SP58) characterised by a foliated granite. (h–j) Exposed AIE-W samples, consisting of multiple granite phases ranging from pink K-feldspar-rich granite to leucogranite. (k–m) Voluminous Steeles Granite comprising multiple granite phases, ranging from porphyritic biotite granite with varying degrees of deformation (k, l) to foliated granodiorite (m). (n–o) Copper Valley Granite, a fine- to medium-grained exhibiting strong foliation (n) and possible associated granitic dyke (o). (p) Sybella granitoid, represented by a fine- to medium-grained granite that is deformed.

proportion of hornblende, but the diorite phase has the largest amount of hornblende with no K-feldspar (Figure 3m). The pluton is also intruded by weakly deformed, medium- to fine-grained felsic dykes that contain a smaller percentage of mafic minerals than the porphyritic phases. Eight samples were collected from the Steeles Granite, two samples from the biotite granite (SP01 and SP22), four samples from the biotite granodiorite (SP24, SP69, SP71 and SP72) and two samples from a felsic dyke (SP02 and SP23).

### *WBIE-CV samples*

The Copper Valley Granite (WBIE-CV) shows evidence of intense deformation and metamorphism displaying a gneissic fabric and migmatites are present locally. Its composition is dominated by a medium-grained gneissic granite consisting of quartz, feldspar and biotite (Figure 3n). The pluton is intruded by weakly deformed dykes having a similar mineralogical composition with the main gneissic granite phase (Figure 3o). Three samples (SP53, SP61 and SP62) were collected from the main phase, and two samples (SP52 and SP65) were collected from a weakly deformed dyke.

### *Sybella Igneous Event (SIE)*

One pluton mapped as Sybella Granite occurs in the southwestern part of the Dajarra region (Figure 2). This pluton intrudes the Alpha Centauri Metamorphics and the Jayah Creek Metabasalt. It is granitic in composition, undeformed to weakly deformed and medium-grained, and consists of quartz, K-feldspar and biotite, with minor sulfide alteration (Figure 3p). Two samples (SP46 and SP47) were collected from this intrusion for analyses.

## Lithogeochemical study

Representative samples were selected for lithogeochemical analysis, as outlined in the previous section. All samples were first processed at the Mineral Separation Laboratory, James Cook University (Australia), where they were split and trimmed to remove weathered or altered surfaces. The prepared samples were then shipped to Bureau Veritas Minerals (Canada) for whole-rock geochemical analysis.

Each sample weighed ~300 g and was submitted for major- and trace-element analysis. Sample preparation followed standard Bureau Veritas protocols. The samples were crushed to achieve >70% of material passing through a 2 mm mesh. A 250 g aliquot of the crushed material was then pulverised such that >85% of the resulting powder was <75 µm in grainsize. Major-element concentrations were analysed by X-ray fluorescence (XRF). For XRF preparation, powdered samples were fused with a lithium borate flux and heated to >1000 °C until completely molten. The melt was subsequently cooled to produce a homogeneous glass disc for XRF measurement. Trace-element concentrations, including rare earth elements (REEs), were determined by inductively coupled plasma-mass spectrometry (ICP-MS). Pulverised samples underwent lithium borate fusion prior to dissolution, ensuring complete breakdown of refractory phases before ICP-MS analysis.

## Results

Whole-rock major- and trace-element data for 33 samples from the Dajarra region are provided in the Supplemental data (Table A2). Interpretation of magma sources, magmatic processes and Paleoproterozoic crustal evolution requires careful consideration of the potential effects of metamorphism and alteration. To minimise these effects, petrogenetic interpretations were derived from relatively immobile major and trace elements.

### *Major elements*

Granitoids from the Dajarra region display lithogeochemical characteristics comparable with other magmatic rocks across the Mount Isa Inlier (Figure 4). They span felsic to highly evolved intermediate compositions, with $SiO_2$ contents ranging from 62.61 to 76.69 wt%. The samples are characterised by low MgO contents (0.01–1.73 wt%), a wide range of $Fe_2O_3^t$ ($Fe_2O_3^t$ = 0.77–9.60 wt%), low to very low $TiO_2$ (0.05–1.29 wt%) and high total alkali contents ($Na_2O + K_2O$ = 5.80–9.25 wt%). On Harker variation diagrams, most major oxides display decreasing trends with increasing $SiO_2$, apart from $K_2O$, which shows a positive correlation (Figure 4). On the total alkali–silica (TAS) diagram, the majority of samples plot within the granodiorite and granite fields, with a small number classified as quartz monzonite (Figure 5a). Most intrusive rocks are ferroan, as indicated by their Fe-index ($FeO^t/[FeO^t + MgO]$; Figure 5b), and exhibit alkalic-calcic to calc-alkalic affinities based on the modified alkali–lime index ($MALI = Na_2O + K_2O - CaO$), with only a few samples showing calcic compositions (Figure 5c). All samples are strongly peraluminous (A/CNK > 1.10), except for the Kalkadoon Granite, which is metaluminous (A/CNK = 0.99; Figure 5d). Because mineralogical descriptions are based mainly on hand-specimen observations, the strongly peraluminous whole-rock compositions should not be taken to imply that the full aluminous mineral budget has been resolved petrographically. For further granite discrimination, the alkali–lime index [$(Na_2O + K_2O)/CaO$] was calculated. The KIE sample has a $(Na_2O + K_2O)/CaO$ ratio of 2.54. The AIE-E samples show $(Na_2O + K_2O)/CaO$ ratios ranging from 1.81 to 11.68, with a mean of 5.22, and those from the AIE-W samples range from 3.44 to 9.24, with an average of 6.88. The WBIE-S samples yield the $(Na_2O + K_2O)/CaO$ ratios between 1.88 and 8.22 (mean = 3.85), while the WBIE-CV samples range from 2.79 to 6.37, with an average value of 4.83. The SIE samples exhibit consistently a $(Na_2O + K_2O)/CaO$ ratio between 6.34 and 6.94 with a mean of 6.64.

### *Trace elements*

The primitive mantle and chondrite-normalised patterns are broadly similar across all samples, although distinct differences can be recognised between individual groups.

The KIE sample exhibits strong enrichment in large ion lithophile elements (LILEs), but overall abundances are systematically lower than those of the other granitoid groups (Figure 6a). The Nb anomaly is relatively weak, K is strongly enriched, and Sr forms a distinctive positive feature relative to neighbouring elements. The Zr–Sm levels are moderate, and the Ti anomaly is present but not extreme. Heavy rare earth elements (HREEs) are moderately depleted, producing a smooth, gently declining pattern. The Kalkadoon Granite exhibits a moderately fractionated REE pattern (Figure 6b), characterised by a weak negative Eu anomaly (Eu/Eu* = 0.77) and depressed HREE concentrations [$(Sm/Yb)_{CN}$ = 5.89]. The 10 000 × Ga/Al ratio is 1.94, and the combined trace-elements concentration (Zr + Nb + Ce + Y) is 455 ppm.

The Argylla granitoids display pronounced compositional differences between samples east (AIE-E) and west (AIE-W) of the Rufus Fault. On the primitive-normalised pattern, the AIE-E samples (Figure 6c) exhibit very strong enrichment in LILEs and light rare earth elements (LREEs), with well-developed Nb and Ti troughs. Zr–Sm are enriched, HREEs are moderately depleted, and Sr is suppressed relative to the Kalkadoon granitoids. Chondrite-normalised REE patterns (Figure 6d) are moderately fractionated [$(La/Yb)_{CN}$ = 5.59–20.62], with negative Eu anomalies (Eu/Eu* = 0.30–0.90) and flat to moderately inclined HREE-depleted slopes [$(Sm/Yb)_{CN}$ = 1.41–3.70]. The 10 000 × Ga/Al ratios range from 1.82 to 3.21, with an average value of 2.51. The combined concentration of Zr + Nb + Ce + Y varies between 125 and 1052 ppm, averaging 605 ppm.

The AIE-W samples display systematically lower absolute enrichment across almost all elements (*e.g.* Rb, Ba, Th, U, K), the deepest Ti trough of all groups, and Sr is very strongly depleted (Figure 6c). The Zr–Sm are strongly suppressed, and the HREEs are the lowest of all samples. Chondrite-normalised REE patterns (Figure 6d) show steep overall slopes but are weakly fractionated [$(La/Yb)_{CN}$ = 2.54–5.72], have low absolute REE

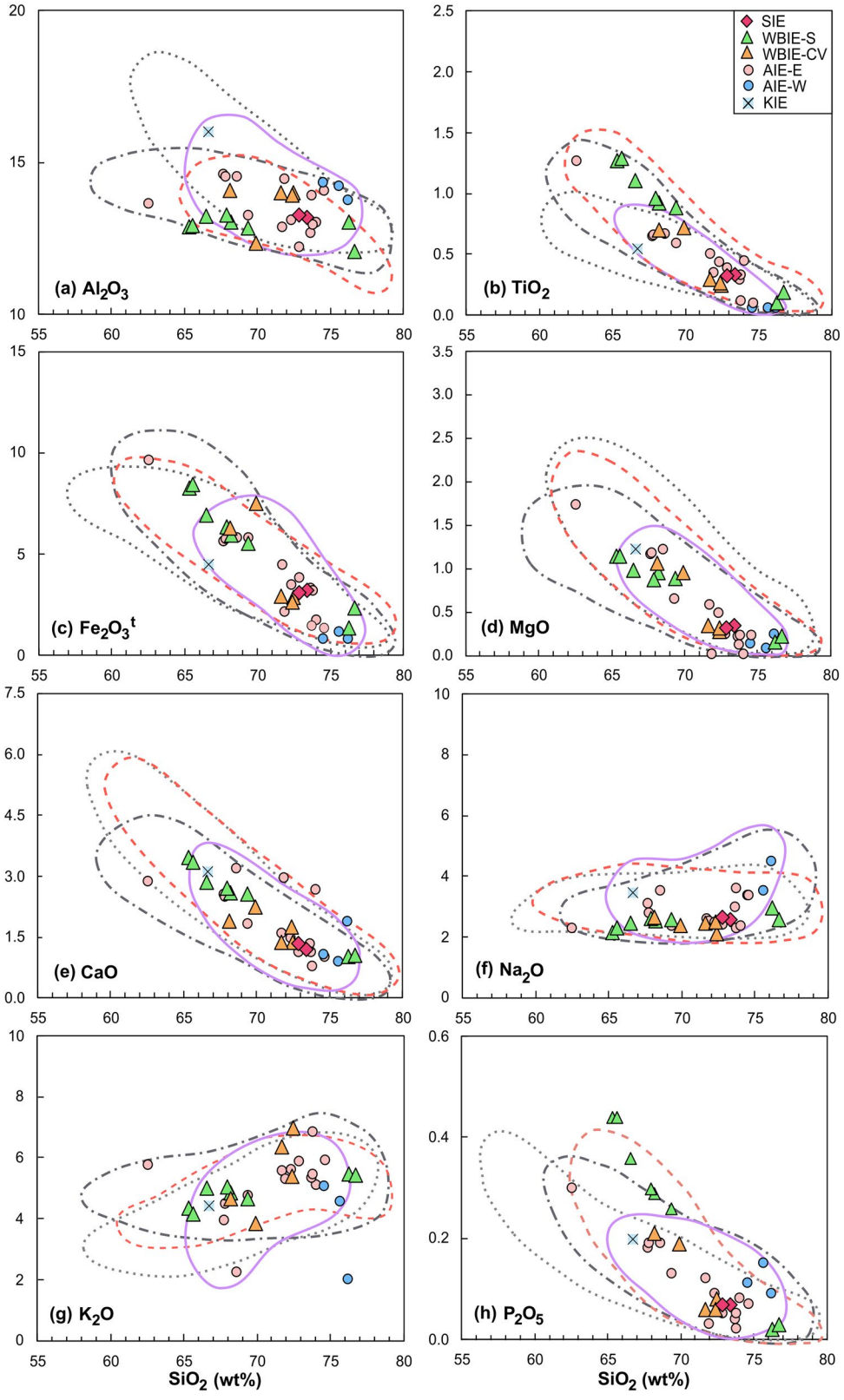


**Figure 4.** Harker variation diagrams for granitoids in the Dajarra region. Granitoids from the Mount Isa Inlier (Supplemental data) are shown as distinct compositional fields: the grey dotted line outlines the Kalkadoon Igneous Event, the purple solid line encloses the Argylla Igneous Event, the dark grey dot–dash line defines the Wonga-Burstall Igneous Event, and the pink dashed line outlines the Sybella Igneous Event.

concentrations, weak Eu anomalies (Eu/Eu* = 0.75–0.79), and flat to weakly inclined HREE segments [$(Sm/Yb)_{CN}$ = 0.65–1.23], forming the most depressed Dy–Lu segment relative to the AIE-E samples. The 10 000 × Ga/Al ratio is 1.34–1.81 with an average of 1.57, the concentration of Zr + Nb + Ce + Y is 62–80 ppm with an average of 71 ppm.

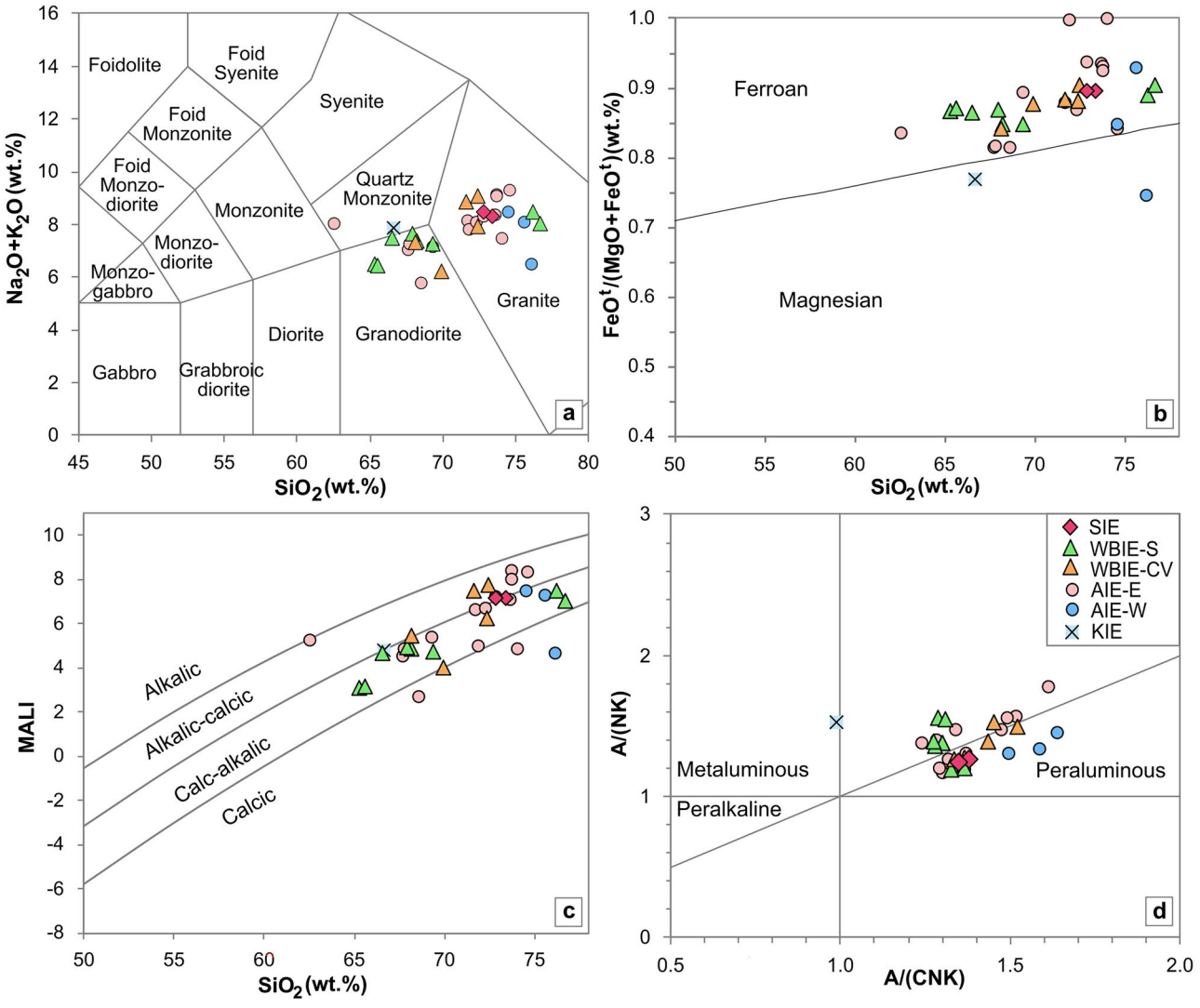


**Figure 5.** Major-element discrimination diagrams for granitoid in the Dajarra region: (a) TAS diagrams (Middlemost, 1994), (b) $SiO_2$ *vs* $FeO^t/(MgO+FeO^t)$ (Frost *et al.*, 2001), (c) $SiO_2$ *vs* MALI (modified alkali-lime index: $Na_2O+K_2O-CaO$) and (d) Shand's index diagram (Maniar & Piccoli, 1989). A/CNK = $Al_2O_3/(CaO+Na_2O+K_2O)$. A/(NK) = $Al_2O_3/(Na_2O+K_2O)$.

The WBIE-S samples are characterised by strong enrichment in LILEs and LREEs, although overall abundances are generally lower than those of the AIE-E and Sybella granitoids (Figure 6e). Primitive mantle-normalised patterns display pronounced Nb and Ti troughs similar to other granitoid groups, together with marked Sr depletion. Zr–Sm are moderately to strongly enriched, whereas HREEs show moderate depletion. Chondrite-normalised REE pattern (Figure 6f) are moderately fractionated [$(La/Yb)_{CN}$ = 10.68–17.51], with clear negative Eu anomalies (Eu/Eu* = 0.3–0.67). The HREE segments are weakly inclined segments [$(Sm/Yb)_{CN}$ = 2.69–3.17], indicating moderate HREE depletion. The 10 000 × Ga/Al ratios range from 2.03 to 2.80, with an average value of 2.40. The combined trace-element parameter (Zr + Nb + Ce + Y) varies between 202 and 1000 ppm, averaging 686 ppm.

The WBIE-CV samples (Figure 6e) have a similar trace-element pattern to AIE-E and SIE samples (Figure 6f, h) displaying a similar Th–U–LREE enrichment, Zr–Sm levels and a comparable Nb anomaly. These samples display a strong Ti anomaly, suppressed Sr concentrations and moderate HREE depletion. Chondrite-normalised REEs (Figure 6f) are moderately to strongly fractionated [$(La/Yb)_{CN}$ = 5.79–71.56] and have moderate Eu anomalies (Eu/Eu* = 0.48–0.58). The HREE segments range from moderately to steeply inclined [$(Sm/Yb)_{CN}$ = 1.85–8.91], indicating stronger HREE depletion relative to the WBIE-S. The 10 000 × Ga/Al ratio is 2.09–2.93 with an average of 2.39, and the concentrations of Zr + Nb + Ce + Y range from 513 to 548 ppm, with an average of 535 ppm.

The SIE samples display the highest overall enrichment in Th–U, LREEs and Zr–Sm. They have very deep Nb and Ti anomalies, and Sr is strongly suppressed (Figure 6g). Compared with the other groups, HREE abundances are relatively elevated but still fractionated. Chondrite-normalised REE patterns (Figure 6h) show strong LREE enrichment [$(La/Yb)_{CN}$ = 12.72–16.96] and

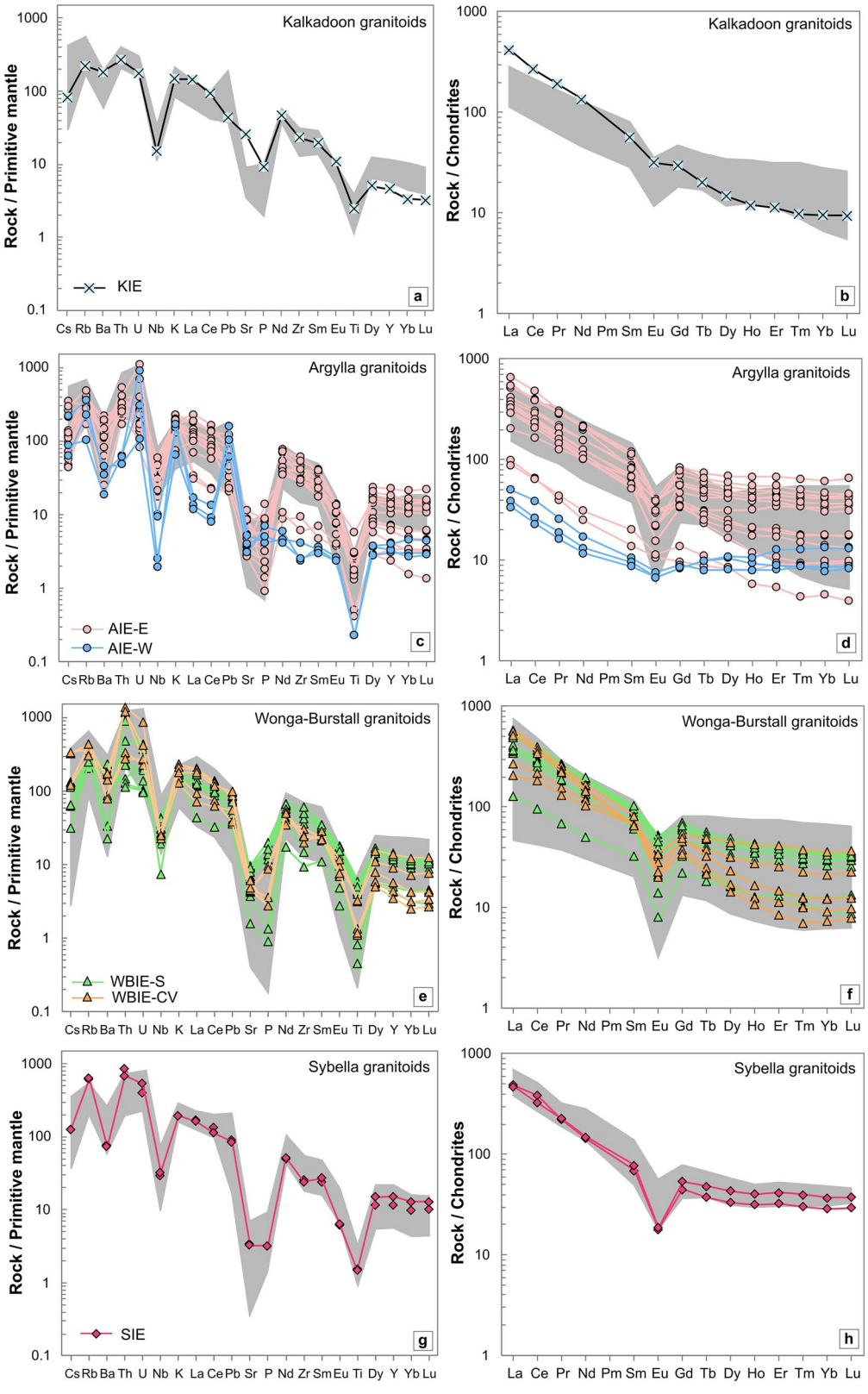


**Figure 6.** Primitive mantle-normalised (a, c, e, g) and chondrite-normalised rare earth element (b, d, f, h) diagrams for granitoids from the Dajarra region. The grey field represents granitoid compositions across the Mount Isa Inlier. Normalisation values are from Sun and McDonough (1989).

well-developed negative Eu anomalies (Eu/Eu* = 0.29–0.32). The HREE segments are flat to weakly inclined [$(Sm/Yb)_{CN}$ = 2.11–2.42] indicating the least HREEs depletion among the analysed granitoid groups. The 10 000 × Ga/Al ratio ranges between 2.55 and 2.60 with an average of 2.57, and the concentration of Zr + Nb + Ce + Y is 560–594 ppm with an average of 577 ppm.

## Discussion

### *Geochemical characteristics and comparison with similar age igneous rocks in Mount Isa Inlier*

Most igneous rocks in the Dajarra region are peraluminous and ferroan, and range from calc-alkalic to alkalic-calcic. They are enriched in LILEs and HFSEs, display pronounced negative Ba, Sr, Eu and Ti anomalies, and show HREE depletion, which are characteristics typical of A-type granites or highly evolved I-type granites (*e.g.* Collins *et al.*, 2020; Condie *et al.*, 2023; Kemp & Hawkesworth, 2003). On typical A-type discrimination diagrams, most samples plot near the boundary between A-type and I- and S-type granites (Figure 7). In this study, zircon saturation thermometry ($T_{Zr}$) is applied to estimate the temperature of felsic magma generation (Figure 8a; Boehnke *et al.*, 2013). Zircon saturation temperatures are sensitive to whole-rock composition through the M parameter [cation ratio; (Na + K + 2Ca)/(Al·Si)] and may be affected by post-emplacement modification (*e.g.* alteration, metamorphism, or crystal accumulation), so the calculated $T_{Zr}$ values should be regarded as first-order estimates. However, some variations between and within the groups are present with implications for their petrogenesis, geochemical affinity and magmatic evolution.

The KIE sample from the Dajarra region is distinct from all other samples and shows geochemical characteristics typical of KIE magmatic rocks in the inlier (Figure 7). This sample is metaluminous, magnesian and calc-alkalic, and falls within the field of I- and S-type granites on the A-type discrimination diagrams. The overall geochemical composition of KIE rocks is consistent with I-type characteristics and include moderate to high $Al_2O_3$ contents, relatively high $Na_2O + CaO$, lower $TiO_2$, Nb, Zr, Th than younger granites in Mount Isa Inlier, enrichment in K, Rb, La, Ce, small negative Eu anomalies and a lack of extreme HFSE depletion (Wyborn, 1988; Wyborn & Page, 1983). These geochemical characteristics are shared by the sample collected from the Kalkadoon granite (Figure 6a, b). In general, the Kalkadoon granites are I-type granitoids, characterised by intracrustal igneous sources, low initial $^{87}Sr/^{86}Sr$ ratios, slightly negative εNd and εHf values, low Cr–Ni–MgO contents, tonalite–granodiorite–monzogranite compositions and hornblende–biotite mineralogy, consistent with melting of an enriched lower-crustal reservoir rather than sedimentary protoliths (Bierlein *et al.*, 2008; Bierlein & Betts, 2004; Noptalung *et al.*, 2026; Wyborn, 1988; Wyborn & Page, 1983).

The AIE-E and AIE-W samples show distinctively different geochemical characteristics (Figure 6c, d) and variations on the A-type granites discrimination diagrams (Figure 7). The AIE-E samples straddle the boundary between A-type and I- and S-type granites, whereas the AIE-W samples plot within the field of I- and S-type granites. Within the AIE-E group, the majority of the samples (SP16, SP32, SP33, SP17, SP20, SP21, SP66, SP67, SP55, SP56) have a strong ferroan composition, very high total HSFE contents (>500–1000 ppm) and very high zircon saturation temperatures ($T_{Zr}$ = 851–966 °C; Figure 8a) typical for A-type granites. The remaining AIE-E samples are either highly fractionated I-type granites or transitional between I- and A-type. In contrast, the AIE-W samples are peraluminous and HFSE-poor, and have low Ga/Al ratios, low zircon saturation temperatures ($T_{Zr}$ = 640–673 °C; Figure 8a) and decreasing $P_2O_5$ with increasing $SiO_2$, which are inconsistent with an A-type character and, combined with the biotite–muscovite mineralogy, suggest an S-type character. The AIE-W samples show similar geochemical characteristics to the Big Toby and Yeldham granites that also crop out west of the Rufus-Mount Isa Fault and were proposed to have an S-type affinity (*e.g.* Wyborn *et al.*, 1988). The Big Toby and Yeldham granites are also peraluminous and have high $K_2O$, $TiO_2$, $Al_2O_3$ and Sr, and low HFSE concentrations (Wyborn *et al.*, 1988). The AIE-E samples, which appear to be geochemically similar to the Argylla Formation volcanics, display an A-type character and are ferroan, have high $TiO_2$, $K_2O$, $P_2O_5$, F and zircon saturation temperature ($T_{Zr}$ average of 952 °C), are enriched in HFSE and LILE and have low $Al_2O_3$ and Sr (*e.g.* Wilson, 1983; Wyborn *et al.*, 1988).

The WBIE-S and WBIE-CV samples are geochemically similar (Figure 6e, f) and will be treated as a single group as part of this discussion. On the A-type granites discrimination diagram (Figure 7), they straddle the boundary between A-type and I- and S-type granites, whereas their geochemical characteristics such as ferroan affinity, strong HFSE and LREE enrichment, moderate negative Eu anomalies, medium to high zircon saturation temperature ($T_{Zr}$ = 759–919 °C; Figure 8a) and low Ga/Al ratios (1.97–2.80) are consistent with highly evolved, ferroan, HFSE-enriched felsic magmas, transitional between I-type and A-type-like compositions, rather than classic calc-alkaline I-type granites. Although the WBIE-S and WBIE-CV are younger than the Wonga-Burstall plutons from the EFB, they share several first-order geochemical similarities. Like Wonga-Burstall granitoids (*e.g.* Wyborn *et al.*, 1988), the WBIE samples from the WFB are high-$SiO_2$, strongly differentiated felsic rocks, showing low to very low Sr, elevated Rb/Sr and systematic decreases in $P_2O_5$ with increasing $SiO_2$, consistent with advanced feldspar- and apatite-controlled fractional crystallisation. They also overlap the Burstall granitoids $SiO_2$ range (~69–77 wt%) and display Zr depletion with differentiation, a feature reported for the Wonga suite and indicative of zircon saturation during late-stage evolution. In addition, the WBIE-S samples show relative F enrichment, broadly consistent with the F-rich character noted for Wonga granitoids. Overall, the WBIE rocks from the WFB have similar highly evolved, Sr-depleted, fractionation-dominated geochemical style characteristic to the Wonga-Burstall magmatic association from the EFB, even though some trace-element trends (*e.g.* Y and Nb) diverge in detail. In contrast, the Weberra granite, which is similar in age to the WBIE plutons from the WFB, shows clear A-type characteristics such as strong enrichment in HFSE, very low Sr, strong negative Eu anomalies, high zircon saturation temperature ($T_{Zr}$ = 883–911 °C) and Ga/Al ratios typical of A-type granites (Wyborn *et al.*, 2001).

The SIE samples of Dajarra region exhibit high $SiO_2$, elevated HFSE–LREE contents (Figure 6g, h) and strong F-enrichment (Figure 8b). However, they illustrate moderate Ga/Al ratios, non-extreme Eu anomalies and HFSE concentrations below canonical A-type thresholds, indicating highly fractionated,

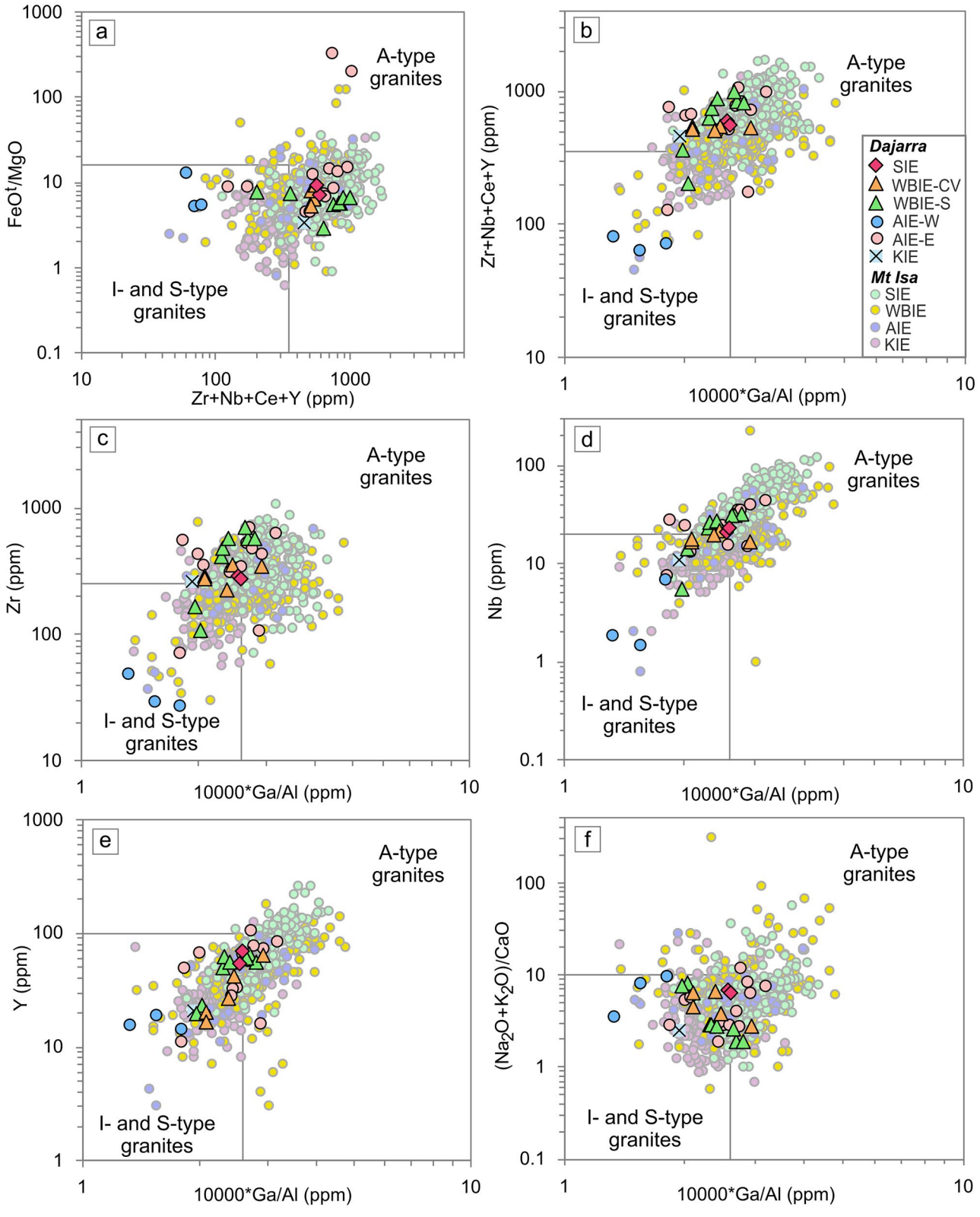


**Figure 7.** Diagrams showing the granite affinities of the granitoids in Mount Isa Inlier and Dajarra region after Whalen *et al.* (1987). (a) FeO$^t$/MgO *vs* Zr + Nb + Ce + Y, (b) Zr + Nb + Ce + Y *vs* 10 000*Ga/Al, (c) Zr *vs* 10 000*Ga/Al, (d) Nb *vs* 10 000*Ga/Al, (e) Y *vs* 10 000*Ga/Al and (f) (Na$_2$O + K$_2$O)/CaO *vs* 10 000*Ga/Al.

F-rich, I-type granites rather than true A-type magmas. The SIE samples closely match the published geochemical characteristics of the Sybella plutons (Wyborn *et al.*, 2001), comprising uniformly high $SiO_2$ felsic compositions with a restricted silica range and strong F enrichment, HFSEs and LREEs, together with elevated Th and U. Low Sr and high Rb contents indicate advanced magmatic differentiation, consistent with the highly evolved nature of Sybella plutons reported from the Mount Isa

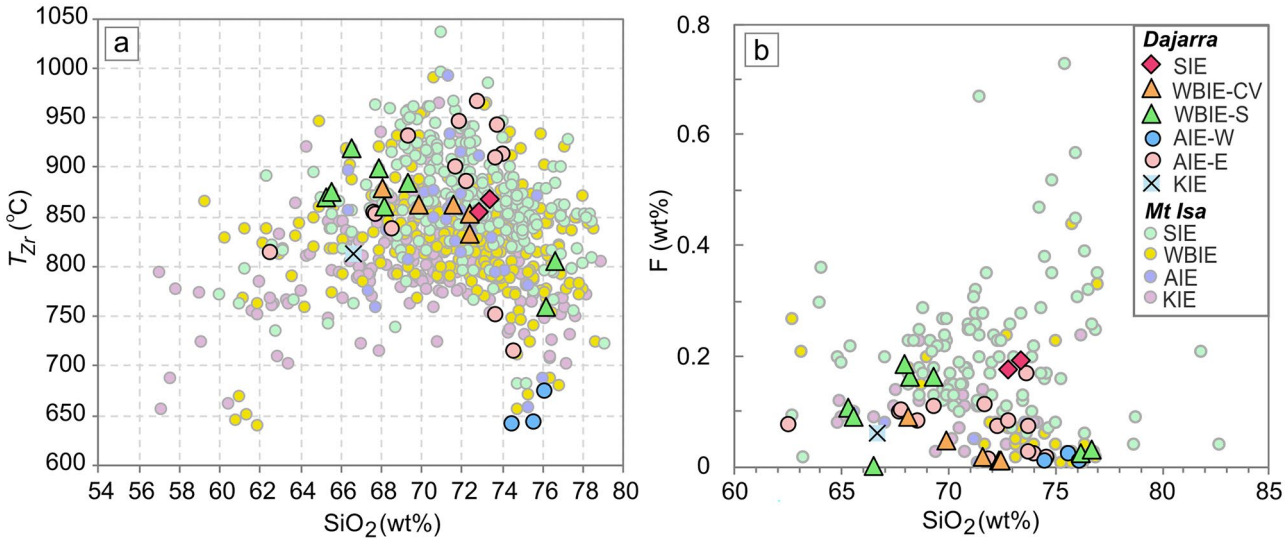


**Figure 8.** Zircon saturation temperatures ($T_{Zr}$) and fluorine (F) enrichment of selected granites from Mount Isa Inlier and Dajarra region. (a) Plot of $T_{Zr}$ (°C) *vs* $SiO_2$ (estimated temperature based on zircon saturation thermometry by Boehnke *et al.*, 2013). (b) Plot of F *vs* $SiO_2$ contents.

Inlier. Despite their enriched trace-element character, the samples display moderate Eu anomalies and Ga/Al ratios below typical A-type thresholds, supporting derivation from fractionated, hydrous I-type magmas rather than primary A-type melts. Accordingly, the SIE samples are best interpreted as typical Sybella-style high-F felsic members, representing late-stage residual melts generated by extensive fractional crystallisation within the Sybella magmatic system.

### *Petrogenesis and tectonic setting*

The interpretation of the petrogenesis and tectonic setting of the igneous rocks from the Dajarra region cannot be separated from the wider evolution of the Mount Isa Inlier and the NAC in general. Moreover, the igneous evolution in the Dajarra region spans *ca* 200 Ma comprising plutons emplaced during the Barramundi Orogeny at *ca* 1850 Ma to the plutons emplaced during the opening of the Calvert Superbasin at *ca* 1665 Ma (Noptalung *et al.*, 2026) spanning multiple igneous and tectonic cycles. Although most samples from this study, except the KIE and AIE-W samples, display A-type like characteristics, such as enriched HFSE and LILE, ferroan composition and high zircon saturation temperature, they have much lower Ga/Al ratios than typical A-type granites and most likely represent transitional magmas between I- and A-type affinities. Following Eby's (1992) classification of A-type granites into $A_1$ and $A_2$ groups, all samples from Dajarra region plot within the group of $A_2$ granites (Figure 9a) derived from continental crust or underplated crust that has been through a cycle of continent–continent collision or island arc magmatism.

The petrogenesis and tectonic setting of crustal derived magmas with A-type characteristics are contentious, and proposed sources include metasedimentary rocks, granulitic residuum from previously extracted I-type magmas and calc-alkaline granitoids such as tonalite and granodiorite (*e.g.* Collins *et al.*, 1982; Frost & Frost, 2011; King *et al.*, 1997; Patiño Douce, 1997; Whalen *et al.*, 1987). Melting experiments of crustal materials have only partially produced magmas with A-type characteristics (*e.g.* Clemens *et al.*, 1986; Creaser *et al.*, 1991; Patiño Douce, 1997), and some involvement of mantle-derived melts is expected, especially to explain the high temperature of A-type melts (*e.g.* Bonin, 2007; Collins, 2002; Frost & Frost, 2011). Because mantle melts are required to explain the high temperature of A-type magmas, most authors favour a tectonic setting involving some form of extension, typically in a back-arc setting or post-orogenic collapse with extension induced by slab rollback or slab tear/failure in which either the crust is thinner, or voluminous mantle melts are emplaced in the lower crust (*e.g.* Bonin *et al.*, 1998; Cui *et al.*, 2022; Grebennikov *et al.*, 2016; Liu *et al.*, 2021). In a review of magmatism resulting from slab failure/slab break-off (high-temperature melting after collision or tectonic reconstruction), Whalen and Hildebrand (2019) proposed that the $A_2$-type granite characteristics such as late- to post-collisional timing, crustal compositions, hot, elevated HFSE and REE ratios link them genetically to slab failure magmas. Since most of the Dajarra samples exhibit a transitional A-type character, they plot across the $A_2$ and slab failure fields on the Whalen and Hildebrand (2019) discrimination diagrams (Figure 9b–d).

The KIE records high-temperature, dominantly I-type magmatism generated by partial melting of pre-existing continental crust. This interpretation is supported by whole-rock Nd, Sr and zircon Hf isotopes, which are mainly dominated by unradiogenic values and favour intense crustal reworking with limited juvenile crust addition during the emplacement of the KIE plutons (*e.g.* Bierlein *et al.*, 2008; Bierlein & Betts, 2004; Noptalung *et al.*, 2026; Olierook *et al.*, 2022; Wyborn & Page, 1983). While early models interpreted this magmatism as intracontinental and heat-driven (Wyborn *et al.*, 1988, 2001), more recent geochronological and isotopic constraints demonstrate that KIE formed within a long-lived active continental margin along the NAC, where subduction-related thermal input promoted

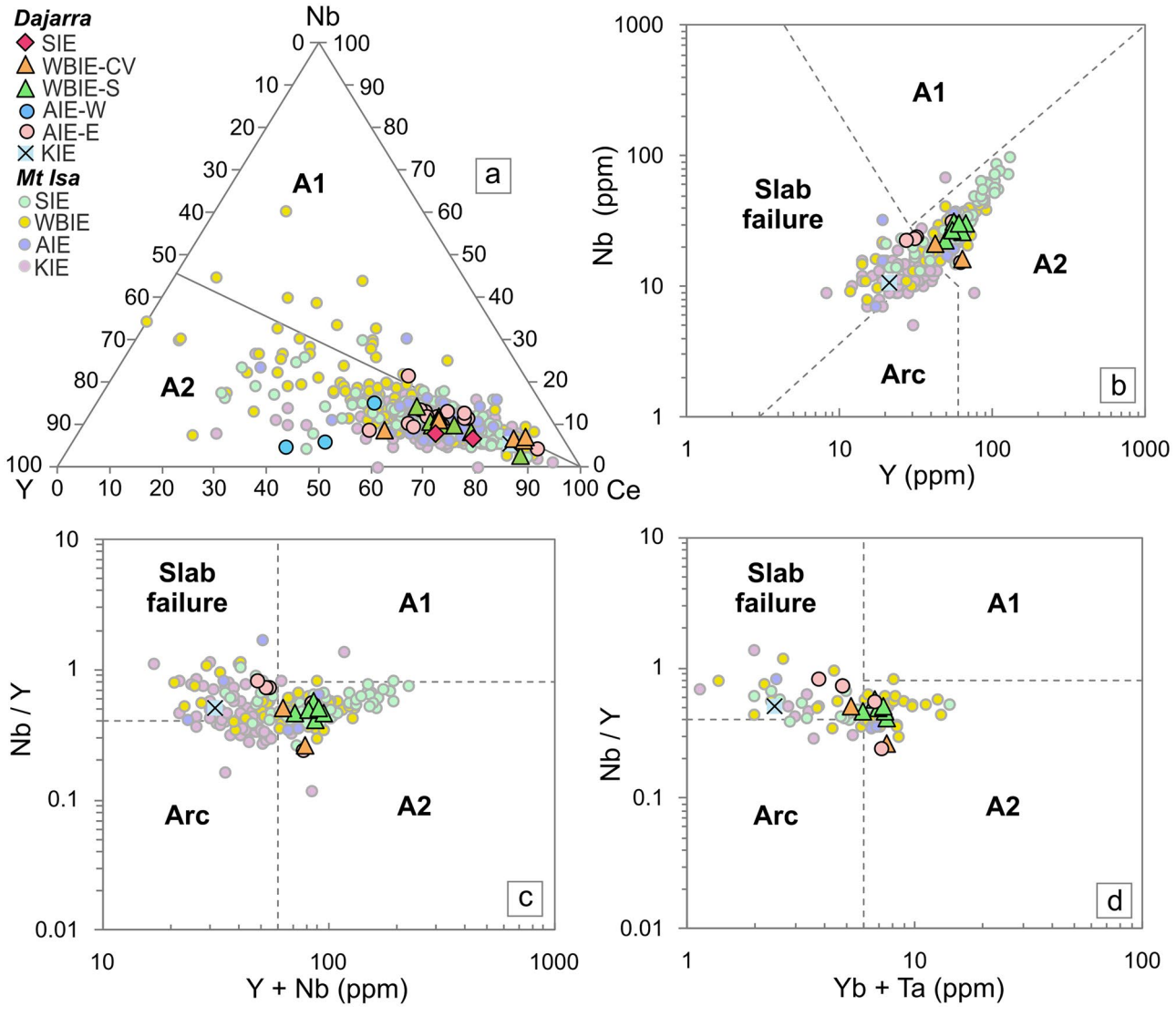


**Figure 9.** Trace-element discrimination diagrams of granitoids from the Mount Isa Inlier and Dajarra region. (a) Ce–Nb–Y diagram by Eby (1992). (b–d) Discrimination plots of arc, slab failure and A-type granitoids by Nb *vs* Y, Nb/Y *vs* Y + Nb and Nb/Y *vs* Yb + Ta (Whalen & Hildebrand, 2019). Using discrimination plots of Whalen and Hildebrand (2019), this required the samples with $SiO_2$ contents between 55 and 70 wt% and an aluminium saturation index (ASI) < 1.1.

extensive crustal reworking during early Nuna assembly (Gibson *et al.*, 2025; Noptalung *et al.*, 2026). The only KIE sample from Dajarra region is within the field of slab-failure magmas (Figure 9b–d), consistent with the emplacement during the terminal stage of the Barramundi Orogeny (Figure 10; Noptalung *et al.*, 2026).

The final stages of the AIE coincide with the opening of the Leichhardt Superbasin and the emplacement of the mafic Eastern Creek Volcanics in the WFB and the felsic Argylla Formation in the EFB. The input of more juvenile, mafic magmas during this period is reflected in the Hf isotopic compositions, which, although dominated by crustal signatures, show positive εHf excursions consistent with mantle input and crustal extension (Noptalung *et al.*, 2026; Olierook *et al.*, 2022). Early interpretations proposed that AIE magmatism represents post-orogenic intracontinental magmatism (*e.g.* Bierlein & Betts, 2004; Wyborn *et al.*, 1988, 2001), whereas latest interpretations (Gibson *et al.*, 2020, 2025; Noptalung *et al.*, 2026) proposed that the AIE formed within an active continental margin system in response to slab rollback, lithospheric thinning and localised mantle input responsible for high-temperature crustal melting. Consequently, the resulting magmas range from fractionated I-type to transitional I–A and classic A-type compositions, most likely reflecting progressive thermal escalation rather than discreet tectonic regimes. Since AIE magmatism occurred during a period of tectonic switching leading into extension and basin development (*e.g.* Leichhardt Superbasin at *ca* 1790 Ma; Figure 10), the AIE samples span across the field of $A_2$ and slab-failure granites on the Whalen and Hildebrand (2019) discrimination diagrams (Figure 9b–d).

The concentration of S-type granitoids west of the Rufus-Mount Isa Fault may reflect the influence of a major crustal boundary in western Dajarra. Korsch and Doublier (2016) emphasised that major crustal boundaries in Australia are deep-seated structures that commonly separate crustal blocks with contrasting structural trends and may not coincide precisely with mapped surface faults. In the Dajarra region, this boundary

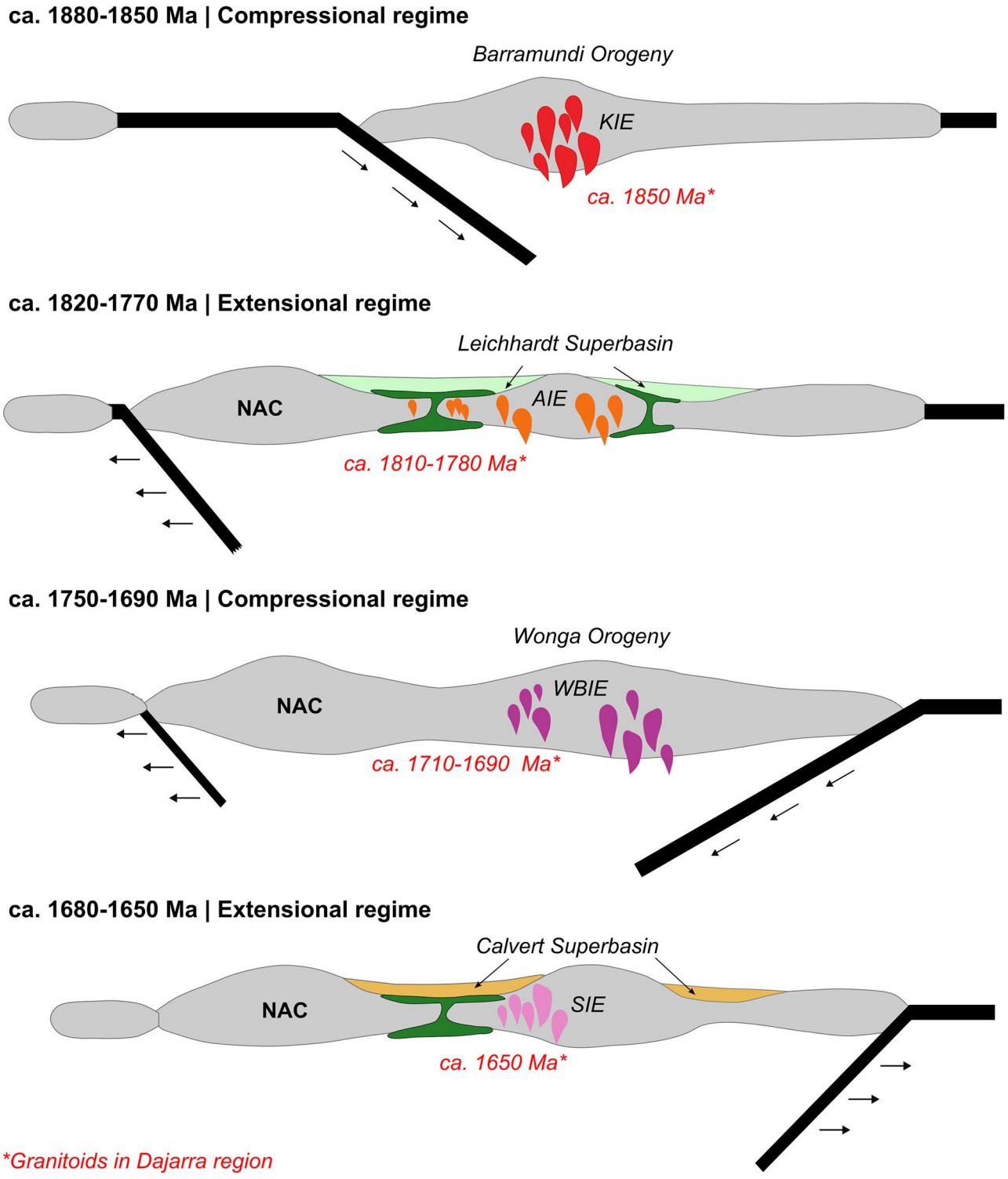


**Figure 10.** Schematic model for the Paleoproterozoic tectonic evolution of the Mount Isa Inlier, illustrating a long-lived convergent margin along the eastern margin of the North Australian Craton (NAC) characterised by episodic switching between compressional and extensional regimes from *ca* 1880 to 1650 Ma. Compression during the Barramundi Orogeny (*ca* 1880–1850 Ma) resulted in crustal thickening and arc-related magmatism, exemplified by emplacement of the Kalkadoon granitoids (KIE). Subsequent extension at *ca* 1820–1770 Ma is interpreted to reflect slab rollback and localised mantle input, coincident with intrusion of the Argylla granitoids (AIE) and development of the Leichhardt Superbasin. Renewed convergence during *ca* 1750–1690 Ma led to crustal shortening associated with the Wonga Orogeny (*ca* 1750–1710 Ma) and emplacement of the Wonga-Burstall granitoids (WBIE); granitoids emplaced at *ca* 1710–1690 Ma mark the onset of slab retreat and initiation of the Calvert Superbasin. Further tectonic switching at *ca* 1680–1650 Ma, linked to continued subduction retreat, resulted in formation of the Calvert Superbasin and emplacement of Sybella magmatism (SIE). Magmatism throughout these stages was dominated by reworking of continental crust, with episodic mantle input during extensional phases.

is consistent with the transition from east–west structural trends in the Northern Territory to north–south trends farther east, along a corridor that follows the Rufus Fault and the western Sybella batholith towards the Mount Oxide domain. This relationship suggests that the western AIE granitoids were emplaced within a structurally distinct crustal domain, which may help explain their S-type affinity relative to the more HFSE-rich granitoids east of the Rufus Fault.

Structural, geochronological and field relationships indicate that the WBIE plutons emplaced between *ca* 1750 and 1710 Ma during the Wonga Orogeny are syn-orogenic (Spence *et al.*, 2021, 2022). However, the WBIE plutons in the Dajarra region were emplaced between *ca* 1710 and 1690 Ma (Noptalung *et al.*, 2026) and thus postdate the Wonga Orogeny. In general, the extracted zircons from WBIE have consistently unradiogenic Hf isotopic compositions (*e.g.* Noptalung *et al.*, 2026; Olierook *et al.*, 2022) indicating minimal juvenile input and dominant melting of a thickened crust consistent with their orogenic character. The younger WBIE plutons from the Dajarra region are also dominated by zircon grains with unradiogenic Hf suggesting minimal to no juvenile input, although a mantle component may be required to explain their relatively high zircon saturation temperature. Most of the WBIE samples from Dajarra region are the $A_2$-type granites (Figure 9) consistent with their strong crustal character indicating melting related to slab rollback during the opening of the Calvert Superbasin (Figure 10).

The SIE samples fall within the $A_2$-type field (Figure 9a), but as discussed above, their overall geochemical characteristics are consistent with highly fractionated, F-enriched (Figure 8b), I-type granites rather than true A-type magmas. Although early interpretations considered SIE granites to be post-orogenic (Wyborn *et al.*, 2001), structural and geochronological constraints demonstrate that magmatism was synchronous with ductile extension along major shear zones (Farquharson & Wilson, 1971; Gibson *et al.*, 2008). The Hf isotopic data of SIE rocks in Dajarra region (Noptalung *et al.*, 2026) indicate minimal juvenile input, implying that SIE magmas formed by partial melting of reworked continental crust. However, further to the north within the main Sybella batholith, mafic endmembers and hybridised intermediate melts have been reported (Hoadley, 2003). This suggests that the overall magmatic evolution during the SIE is more complex than reflected in the samples from the Dajarra region. The SIE magmatism is synchronous with the opening of the Calvert Superbasin and thus marking tectonic switching from contraction during the Wonga Orogeny to extension within a long-lived convergent margin system (Figure 10).

## Conclusions

Granitic intrusions in the Dajarra region record a prolonged history of Paleoproterozoic magmatism along the eastern margin of the NAC, spanning *ca* 200 Ma and encompassing the Kalkadoon, Argylla, Wonga-Burstall and Sybella igneous events. To constrain their geochemical characteristics, petrogenesis and tectonic setting, 33 samples from plutons and associated dykes were selected for lithogeochemical analysis, with major and trace elements measured using XRF and ICP-MS.

The Paleoproterozoic granitoids are highly felsic ($SiO_2 \approx$ 63–77 wt%) with low MgO and $TiO_2$ contents and high total alkalis. These granitic rocks illustrate systematic decreases in most major oxides with increasing $SiO_2$, except for $K_2O$, which exhibits a positive correlation. The intrusions are predominantly ferroan, range from alkalic-calcic to calc-alkalic and are strongly peraluminous, whereas the KIE sample is metaluminous. Trace-element signatures are marked by enrichment in LILEs and HFSEs, with pronounced negative Ba, Sr, Eu and Ti anomalies, and moderately to strongly fractionated REE patterns. Geochemical variations are evident between magmatic suites and across major structural boundaries, particularly between AIE samples east (AIE-E) and west (AIE-W) of the Rufus Fault. AIE-W samples are HFSE-poor with low zircon saturation temperatures, indicative of S-type affinities, whereas AIE-E samples, along with WBIE and SIE samples, show elevated HFSE and higher zircon saturation temperatures.

Granite discrimination diagrams indicate that the representative samples occupy the transitional field between I- and A-type granites and predominantly fall within the $A_2$-type field, suggesting derivation from reworked continental crust. It could imply that magmatism in the Dajarra region was dominated by partial melting of continental crust, with episodic mantle input required to attain high melt temperatures. Based on their geochemical signatures and inferred magma sources, the Paleoproterozoic granitoids of the Dajarra region were emplaced in a subduction-related tectonic setting. This interpretation is consistent with a long-lived convergent margin setting that controlled basin development and orogenic events in the Mount Isa Inlier and broadly coincides with the final assembly of Nuna.

## Acknowledgements

This manuscript forms part of the PhD research conducted by the first author, Sutthida Noptalung, at James Cook University, who was supported by a scholarship from the Institute for the Promotion of Teaching Science and Technology (Thailand). We also thank the reviewers, Laurie Hutton and Nicholas Tailby, for their constructive reviews and insightful comments, which have improved the manuscript.

## Author contributions

CRediT: **S. Noptalung**: Conceptualization, Data curation, Visualization, Writing – original draft; **I. V. Sanislav**: Conceptualization, Supervision, Validation, Writing – review & editing; **H. A. Cocker**: Validation, Writing – review & editing; **A. A. Kumar**: Validation, Writing – review & editing; **M. Sami**: Writing - review & editing.

## Disclosure statement

No potential conflict of interest was reported by the authors.

## Funding

The authors acknowledge funding support from the Economic Geology Research Centre (EGRU) at James Cook University (Townsville, Australia).

## ORCID

S. Noptalung http://orcid.org/0009-0005-5018-0227
I. V. Sanislav http://orcid.org/0000-0002-3680-3740
H. A. Cocker http://orcid.org/0000-0002-5543-5701
A. A. Kumar http://orcid.org/0000-0001-7604-8949
M. Sami http://orcid.org/0000-0002-0567-6283

## Data availability statement

Noptalung, Sutthida; Sanislav, Ioan; Cocker, Helen (2026): Tectonic Switching within a long-lived convergent margin: Evidence from the geochemistry of Paleoproterozoic granitoids, Dajarra region, Mount Isa Inlier. James Cook University. https://doi.org/10.25903/286k-ze14. CC BY 4.0: Attribution 4.0 International.

## References

Abu Sharib, A. S. A. A., & Sanislav, I. V. (2013). Polymetamorphism accompanied switching in horizontal shortening during Isan Orogeny: Example from the Eastern Fold Belt, Mount Isa Inlier, Australia. *Tectonophysics*, *587*, 146–167. https://doi.org/10.1016/j.tecto.2012.06.051

Bagas, L., Bierlein, F. P., Anderson, J. A. C., & Maas, R. (2010). Collision-related granitic magmatism in the Granites–Tanami Orogen, Western Australia. *Precambrian Research*, *177*(1-2), 212–226. https://doi.org/10.1016/j.precamres.2009.12.002

Betts, P. G., & Giles, D. (2006). The 1800–1100 Ma tectonic evolution of Australia. *Precambrian Research*, *144*(1-2), 92–125. https://doi.org/10.1016/j.precamres.2005.11.006

Betts, P. G., Giles, D., Mark, G., Lister, G. S., Goleby, B. R., & Aillères, L. (2006). Synthesis of the Proterozoic evolution of the Mt Isa Inlier. *Australian Journal of Earth Sciences*, *53*(1), 187–211. https://doi.org/10.1080/08120090500434625

Bierlein, F. P., & Betts, P. G. (2004). The Proterozoic Mount Isa Fault Zone, northeastern Australia: Is it really a ca. 1.9 Ga terrane-bounding suture? *Earth and Planetary Science Letters*, *225*(3–4), 279–294. https://doi.org/10.1016/j.epsl.2004.06.022

Bierlein, F. P., Black, L. P., Hergt, J., & Mark, G. (2008). Evolution of Pre-1.8 Ga basement rocks in the western Mt Isa Inlier, northeastern Australia—insights from SHRIMP U–Pb dating and *in-situ* Lu–Hf analysis of zircons. *Precambrian Research*, *163*(1–2), 159–173. https://doi.org/10.1016/j.precamres.2007.08.017

Bierlein, F. P., Maas, R., & Woodhead, J. (2011). Pre-1.8 Ga tectono-magmatic evolution of the Kalkadoon–Leichhardt Belt: Implications for the crustal architecture and metallogeny of the Mount Isa Inlier, northwest Queensland, Australia. *Australian Journal of Earth Sciences*, *58*(8), 887–915. https://doi.org/10.1080/08120099.2011.571286

Blake, D. H. (1986). Middle Proterozoic evolution of the Mt Isa Inlier, north-western Queensland, Australia: A synthesis. *South African Journal of Geology*, *89*(2), 253–262. https://doi.org/10.10520/EJC-1bb4fbcf12

Blake, D. H., & Stewart, A. J. (1992). Stratigraphic and tectonic framework, Mount Isa Inlier. In A. J. Stewart & D. H. Blake (Eds.), *Detailed studies of the Mount Isa Inlier* (pp. 1–11). Australian Geological Survey Organisation Bulletin. 243 p.

Boehnke, P., Watson, E. B., Trail, D., Harrison, T. M., & Schmitt, A. K. (2013). Zircon saturation re-revisited. *Chemical Geology*, *351*, 324–334. https://doi.org/10.1016/j.chemgeo.2013.05.028

Bonin, B. (2007). A-type granites and related rocks: Evolution of a concept, problems and prospects. *Lithos*, *97*(1–2), 1–29. https://doi.org/10.1016/j.lithos.2006.12.007

Bonin, B., Azzouni-Sekkal, A., Bussy, F., & Ferrag, S. (1998). Alkali-calcic and alkaline post-orogenic (PO) granite magmatism: Petrologic constraints and geodynamic settings. *Lithos*, *45*(1-4), 45–70. https://doi.org/10.1016/S0024-4937(98)00025-5

Brown, A., Spandler, C., & Blenkinsop, T. G. (2023). New age constraints for the Tommy Creek Domain of the Mount Isa Inlier, Australia. *Australian Journal of Earth Sciences*, *70*(3), 358–374. https://doi.org/10.1080/08120099.2023.2171124

Bultitude, R. J., Purdy, D. J., Brown, D. D., & Hoy, D. (2021). *Igneous geology of the Mary Kathleen Domain (MKD)* (Queensland Geological Record 2021/02). Geological Survey of Queensland.

Carson, C. J., Hutton, L. J., Withnall, I. W., & Perkins, W. G. (2009). *Joint GSQ-GA NGA geochronology project, Mount Isa region, 2007–2008* (Queensland Geological Record 2008/05). Geological Survey of Queensland.

Claoué-Long, J., & Edgoose, C. (2008). The age and significance of the Ngadarunga Granite in Proterozoic central Australia. *Precambrian Research*, *166*(1-4), 219–229. https://doi.org/10.1016/j.precamres.2007.06.026

Claoué-Long, J., Edgoose, C., & Worden, K. (2008). A correlation of Aileron Province stratigraphy in central Australia. *Precambrian Research*, *166*(1-4), 230–245. https://doi.org/10.1016/j.precamres.2007.06.022

Claoué-Long, J., Maidment, D., Hussey, K., & Huston, D. (2008). The duration of the Strangways Event in central Australia: Evidence for prolonged deep crust processes. *Precambrian Research*, *166*(1-4), 246–262. https://doi.org/10.1016/j.precamres.2007.06.023

Clemens, J. D., Holloway, J. R., & White, A. J. R. (1986). Origin of an A-type granite; experimental constraints. *American Mineralogist*, *71*(3–4), 317–324.

Cocker, H. A., Sanislav, I., Dirks, P., & McCoy-West, A. (2025). Zircon U–Pb emplacement ages of intrusions in the Mary Kathleen Domain, Mount Isa Inlier, Australia. *Australian Journal of Earth Sciences*, *72*(4), 503–527. https://doi.org/10.1080/08120099.2025.2527816

Collins, W. J. (2002). Nature of extensional accretionary orogens. *Tectonics*, *21*(4), 6-1–6-12. https://doi.org/10.1029/2000TC001272

Collins, W. J., Beams, S. D., White, A. J. R., & Chappell, B. W. (1982). Nature and origin of A-type granites with particular reference to southeastern Australia. *Contributions to Mineralogy and Petrology*, *80*(2), 189–200. https://doi.org/10.1007/BF00374895

Collins, W. J., Huang, H.-Q., Bowden, P., & Kemp, A. I. S. (2020). Repeated S–I–A-type granite trilogy in the Lachlan Orogen and geochemical contrasts with A-type granites in Nigeria: Implications for petrogenesis and tectonic discrimination. *Geological Society, London, Special Publications*, *491*(1), 53–76. https://doi.org/10.1144/SP491-2018-159

Collins, W. J., & Shaw, R. D. (1995). Geochronological constraints on orogenic events in the Arunta Inlier: A review. *Precambrian Research*, *71*(1–4), 315–346. https://doi.org/10.1016/0301-9268(94)00067-2

Condie, K. C., Pisarevsky, S. A., Puetz, S. J., Roberts, N. M. W., & Spencer, C. J. (2023). A-type granites in space and time: Relationship to the supercontinent cycle and mantle events. *Earth and Planetary Science Letters*, *610*, 118125. https://doi.org/10.1016/j.epsl.2023.118125

Connors, K. A., & Page, R. W. (1995). Relationships between magmatism, metamorphism and deformation in the western Mount Isa Inlier, Australia. *Precambrian Research*, *71*(1–4), 131–153. https://doi.org/10.1016/0301-9268(94)00059-Z

Creaser, R. A., Price, R. C., & Wormald, R. J. (1991). A-type granites revisited: Assessment of a residual-source model. *Geology*, *19*(2), 163–166. https://doi.org/10.1130/0091-7613(1991)019%253C0163:ATGRAO%253E2.3.CO;2

Cui, X., Sun, M., & Zhao, G. (2022). Syn-orogenic A-type granites and post-collisional I-type granites in the southern Chinese Altai: Petrogenesis and implications for granite classification. *Gondwana Research*, *111*, 20–34. https://doi.org/10.1016/j.gr.2022.07.007

Derrick, G. M. (1982). A Proterozoic rift zone at Mount Isa, Queensland, and implications for mineralisation. *BMR Journal of Australian Geology and Geophysics*, *7*(2), 81–92.

Dutch, R., Hand, M., & Kinny, P. D. (2008). High-grade Paleoproterozoic reworking in the southeastern Gawler Craton, South Australia. *Australian Journal of Earth Sciences*, *55*(8), 1063–1081. https://doi.org/10.1080/08120090802266550

Eby, G. N. (1992). Chemical subdivision of the A-type granitoids: Petrogenetic and tectonic implications. *Geology*, *20*(7), 641–644. https://doi.org/10.1130/0091-7613(1992)020

Etheridge, M. A., Rutland, R. W. R., & Wyborn, L. A. (1987). Orogenesis and tectonic process in the Early to Middle Proterozoic of northern Australia. In A. Kröner (Ed.), *Proterozic Lithospheric Evolution* (pp. 131–147). American Geophysical Union Geodynamics Series 17. https://doi.org/10.1029/GD017p0131.

Farquharson, R. B., & Wilson, C. J. L. (1971). Rationalization of geochronology and structure at Mount Isa. *Economic Geology*, *66*(4), 574–582. https://doi.org/10.2113/gsecongeo.66.4.574

Frost, B. R., Barnes, C. G., Collins, W. J., Arculus, R. J., Ellis, D. J., & Frost, C. D. (2001). A Geochemical Classification for Granitic Rocks. *Journal of Petrology*, *42*(11), 2033–2048. https://doi.org/10.1093/petrology/42.11.2033

Frost, C. D., & Frost, B. R. (2011). On ferroan (A-type) granitoids: Their compositional variability and modes of origin. *Journal of Petrology*, *52*(1), 39–53. https://doi.org/10.1093/petrology/egq070

Gibson, G. M., Champion, D. C., & Doublier, M. P. (2025). The Paleoproterozoic Trans-Australian Orogen: Its magmatic and tectonothermal record, links to northern Laurentia, and implications for supercontinent assembly. *Geological Society of America Bulletin*, *137*(1–2), 495–521. https://doi.org/10.1130/B36255.1

Gibson, G. M., Champion, D. C., Huston, D. L., & Withnall, I. W. (2020). Orogenesis in Paleo-Mesoproterozoic Eastern Australia: A response to arc-continent and continent-continent collision during assembly of the Nuna Supercontinent. *Tectonics*, *39*(2), e2019TC005717. https://doi.org/10.1029/2019TC005717

Gibson, G. M., Henson, P. A., Neumann, N. L., Southgate, P. N., & Hutton, L. J. (2012). Paleoproterozoic–earliest Mesoproterozoic basin evolution in the Mount Isa region, northern Australia and implications for reconstructions of the Nuna and Rodinia supercontinents. *Episodes*, *35*(1), 131–141. https://doi.org/10.18814/epiiugs/2012/v35i1/012

Gibson, G. M., Meixner, A. J., Withnall, I. W., Korsch, R. J., Hutton, L. J., Jones, L. E. A., Holzschuh, J., Costelloe, R. D., Henson, P. A., & Saygin, E. (2016). Basin architecture and evolution in the Mount Isa mineral province, northern Australia: Constraints from deep seismic reflection profiling and implications for ore genesis. *Ore Geology Reviews*, *76*, 414–441. https://doi.org/10.1016/j.oregeorev.2015.07.013

Gibson, G. M., Rubenach, M. J., Neumann, N. L., Southgate, P. N., & Hutton, L. J. (2008). Syn- and post-extensional tectonic activity in the Palaeoproterozoic sequences of Broken Hill and Mount Isa and its bearing on reconstructions of Rodinia. *Precambrian Research*, *166*(1–4), 350–369. https://doi.org/10.1016/j.precamres.2007.05.005

Giles, D., Betts, P., & Lister, G. (2002). Far-field continental backarc setting for the 1.80–1.67 Ga basins of northeastern Australia. *Geology*, *30*(9), 823–826. https://doi.org/10.1130/0091-7613(2002)030%253C0823:FFCBSF%253E2.0.CO;2

Grebennikov, A. V., Khanchuk, A. I., Gonevchuk, V. G., & Kovalenko, S. V. (2016). Cretaceous and Paleogene granitoid suites of the Sikhote-Alin area (Far East Russia): Geochemistry and tectonic implications. *Lithos*, *261*, 250–261. https://doi.org/10.1016/j.lithos.2015.12.020

Hand, M., & Buick, I. S. (2001). Tectonic evolution of the Reynolds–Anmatjira Ranges: A case study in terrain reworking from the Arunta Inlier, central Australia. In J. A. Miller, R. E. Holdsworth, I. S. Buick, & M. Hand (Eds.), *Continental reactivation and reworking* (pp. 237–260). Geological Society of London Special Publication 248. https://doi.org/10.1144/GSL.SP.2001.184.01.12

Hand, M., Reid, A., & Jagodzinski, L. (2007). Tectonic Framework and Evolution of the Gawler Craton, Southern Australia. *Economic Geology*, *102*(8), 1377–1395. https://doi.org/10.2113/gsecongeo.102.8.1377

Hoadley, E. (2003). *Evolution of the Sybella Batholith: Petrographic, geochemical and structural development of an A-type intrusive complex, Northwest Queensland* [unpublished Doctoral thesis]. James Cook University. https://researchonline.jcu.edu.au/1346/

Iaccheri, L. M. (2019). Composite basement along the southern margin of the North Australian Craton: Evidence from in-situ zircon U-Pb-O-Hf and whole-rock Nd isotopic compositions. *Lithos*, *324-325*, 733–746. https://doi.org/10.1016/j.lithos.2018.11.006

Kemp, A. I. S, & Hawkesworth, C. J (2003). 3.11—Granitic perspectives on the generation and secular evolution of the continental crust. In H. D. Holland & K. K. Turekian (Eds.), *Treatise on geochemistry* (pp. 349–410). Pergamon. https://doi.org/10.1016/B0-08-043751-6/03027-9

King, P. L., White, A. J. R., Chappell, B. W., & Allen, C. M. (1997). Characterization and origin of aluminous A-type granites from the Lachlan Fold Belt, southeastern Australia. *Journal of Petrology*, *38*(3), 371–391. https://doi.org/10.1093/petroj/38.3.371

Korsch, R. J., & Doublier, M. P. (2016). Major crustal boundaries of Australia, and their significance in mineral systems targeting. *Ore Geology Reviews*, *76*, 211–228. https://doi.org/10.1016/j.oregeorev.2015.05.010

Korsch, R. J., Huston, D. L., Henderson, R. A., Blewett, R. S., Withnall, I. W., Fergusson, C. L., Collins, W. J., Saygin, E., Kositcin, N., Meixner, A. J., Chopping, R., Henson, P. A., Champion, D. C., Hutton, L. J., Wormald, R., Holzschuh, J., & Costelloe, R. D. (2012). Crustal architecture and geodynamics of North Queensland, Australia: Insights from deep seismic reflection profiling. *Tectonophysics*, *572–573*, 76–99. https://doi.org/10.1016/j.tecto.2012.02.022

Lambeck, A., Barovich, K., Gibson, G., Huston, D., & Pisarevsky, S. (2012). An abrupt change in Nd isotopic composition in Australian basins at 1655 Ma: Implications for the tectonic evolution of Australia and its place in NUNA. *Precambrian Research*, *208–211*, 213–221. https://doi.org/10.1016/j.precamres.2012.01.009

Le, T. X., Dirks, P. H. G. M., Sanislav, I. V., Huizenga, J. M., Cocker, H. A., & Manestar, G. N. (2021a). Geochronological constraints on the geological history and gold mineralization in the Tick Hill region, Mt Isa Inlier. *Precambrian Research*, *366*, 106422. https://doi.org/10.1016/j.precamres.2021.106422

Le, T. X., Dirks, P. H. G. M., Sanislav, I. V., Huizenga, J. M., Cocker, H. A., & Manestar, G. N. (2021b). Geological setting and mineralization characteristics of the Tick Hill Gold Deposit, Mount Isa Inlier, Queensland, Australia. *Ore Geology Reviews*, *137*, 104288. https://doi.org/10.1016/j.oregeorev.2021.104288

Le, T. X., Dirks, P. H. G. M., Sanislav, I. V., Huizenga, J. M., Cocker, H. A., & Nguyen, G. T. T. (2024). *P – T* conditions of metamorphic and hydrothermal events at Tick Hill gold deposit, Mount Isa, Queensland, Australia. *Australian Journal of Earth Sciences*, *71*(4), 538–552. https://doi.org/10.1080/08120099.2024.2320195

Liu, C., Zhao, G., Liu, F., & Xu, W. (2021). Coexistence of A- and I-type granites in the Lüliang Complex: Tectonic implications for the middle Paleoproterozoic Trans-North China Orogen, North China Craton. *Lithos*, *380–381*, 105875. https://doi.org/10.1016/j.lithos.2020.105875

MacCready, T., Goleby, B. R., Goncharov, A., Drummond, B. J., & Lister, G. S. (1998). A framework of overprinting orogens based on interpretation of the Mount Isa deep seismic transect. *Economic Geology*, *93*(8), 1422–1434. https://doi.org/10.2113/gsecongeo.93.8.1422

Magee, C. W., Withnall, I. W., Hutton, L. J., Perkins, W. J., Donchak, P. J. T., Parson, A., Blake, P. R., Sweet, I. P., & Carson, C. J. (2012). *Joint GSQ–GA geochronology project, Mount Isa Region, 2008–2009* (Queensland Geological Record 2012/07). Geological Survey of Queensland..

Maniar, P. D., & Piccoli, P. M. (1989). Tectonic discrimination of granitoids. *Geological Society of America Bulletin*, *101*(5), 635–643. https://doi.org/10.1130/0016-7606(1989)101%253C0635:TDOG%253E2.3.CO;2

Middlemost, E. A. K. (1994). Naming materials in the magma/igneous rock system. *Earth-Science Reviews*, *37*(3–4), 215–224. https://doi.org/10.1016/0012-8252(94)90029-9

Noptalung, S., Sanislav, I. V., Cocker, H. A., & Kumar, A. (2026). Zircon U-Pb ages and Lu-Hf isotopic systematics in granites from Mt Isa Inlier – evidence of prolonged reworking of an active continental margin during the final assembly of the Nuna (Columbia) supercontinent. *Precambrian Research*, *432*, 107965. https://doi.org/10.1016/j.precamres.2025.107965

O'Dea, M. G., Lister, G. S., Betts, P. G., & Pound, K. S. (1997a). A shortened intraplate rift system in the Proterozoic Mount Isa terrane, NW Queensland, Australia. *Tectonics*, *16*(3), 425–441. https://doi.org/10.1029/96TC03276

O'Dea, M. G., Lister, G. S., MacCready, T., Betts, P. G., Oliver, N. H. S., Pound, K. S., Huang, W., & Valenta, R. K. (1997b). Geodynamic evolution of the Proterozoic Mount Isa terrain. In J.-P. Burg & M. Ford (Eds.), *Orogeny through time* (pp. 99–122). Special Publications 121. https://doi.org/10.1144/gsl.sp.1997.121.01.05

Olierook, H. K. H., Mervine, E. M., Armstrong, R., Duckworth, R., Evans, N. J., McDonald, B., Kirkland, C. L., Shantha Kumara, A., Wood, D. G., Cristall, J., Jhala, K., Stirling, D. A., Friedman, I., & McInnes, B. I. A. (2022). Uncovering the Leichhardt Superbasin and Kalkadoon-Leichhardt Complex in the southern Mount Isa Terrane, Australia. *Precambrian Research*, *375*, 106680. https://doi.org/10.1016/j.precamres.2022.106680

Page, R. W. (1983). Timing of superposed volcanism in the Proterozoic Mount Isa Inlier, Australia. *Precambrian Research*, *21*(3–4), 223–245. https://doi.org/10.1016/0301-9268(83)90042-6

Page, R. W., Griffin, T. J., Tyler, I. M., & Sheppard, S. (2001). Geochronological constraints on tectonic models for Australian Palaeoproterozoic high-K granites. *Journal of the Geological Society*, *158*(3), 535–545. https://doi.org/10.1144/jgs.158.3.535

Page, R. W., & Williams, I. S. (1988). Age of the barramundi orogeny in northern Australia by means of ion microprobe and conventional U-Pb zircon studies. *Precambrian Research*, *40–41*, 21–36. https://doi.org/10.1016/0301-9268(88)90059-9

Passchier, C. W., & Williams, P. R. (1989). Proterozoic extensional deformation in the Mount Isa Inlier, Queensland, Australia. *Geological Magazine*, *126*(1), 43–53. https://doi.org/10.1017/S0016756800006130

Patiño Douce, A. E. (1997). Generation of metaluminous A-type granites by low-pressure melting of calc-alkaline granitoids. *Geology*, *25*(8), 743–746. https://doi.org/10.1130/0091-7613(1997)025%253C0743:GOMAT-G%253E2.3.CO;2

Reid, A. J., & Hand, M. (2012). Mesoarchean to Mesoproterozoic evolution of the southern Gawler Craton, South Australia. *Episodes*, *35*(1), 216–225. https://doi.org/10.18814/epiiugs/2012/v35i1/021

Reid, A. J., McAvaney, S. O., & Fraser, G. L. (2008). Nature of the Kimban Orogeny across northern Eyre Peninsula. *MESA Journal*, *51*, 25–34.

Scott, D. L., Rawlings, D. J., Page, R. W., Tarlowski, C. Z., Idnurm, M., Jackson, M. J., & Southgate, P. N. (2000). Basement framework and geodynamic evolution of the Palaeoproterozoic superbasins of north-central Australia: An integrated review of geochemical, geochronological and geophysical data. *Australian Journal of Earth Sciences*, *47*(3), 341–380. https://doi.org/10.1046/j.1440-0952.2000.00793.x

Spence, J. S., Sanislav, I. V., & Dirks, P. H. G. M. (2021). 1750–1710 Ma deformation along the eastern margin of the North Australia Craton. *Precambrian Research*, *353*, 106019. https://doi.org/10.1016/j.precamres.2020.106019

Spence, J. S., Sanislav, I. V., & Dirks, P. H. G. M. (2022). Evidence for a 1750–1710 Ma orogenic event, the Wonga Orogeny, in the Mount Isa Inlier, Australia: Implications for the tectonic evolution of the North Australian Craton and Nuna Supercontinent. *Precambrian Research*, *369*, 106510. https://doi.org/10.1016/j.precamres.2021.106510

Sun, S.-S., & McDonough, W. F. (1989). Chemical and isotopic systematics of oceanic basalts: Implications for mantle composition and processes. *Geological Society, London, Special Publications*, *42*, 313–345. https://doi.org/10.1144/GSL.SP.1989.042.01.19

Whalen, J. B., Currie, K. L., & Chappell, B. W. (1987). A-type granites: Geochemical characteristics, discrimination and petrogenesis. *Contributions to Mineralogy and Petrology*, *95*(4), 407–419. https://doi.org/10.1007/BF00402202

Whalen, J. B., & Hildebrand, R. S. (2019). Trace element discrimination of arc, slab failure, and A-type granitic rocks. *Lithos*, *348–349*, 105179. https://doi.org/10.1016/j.lithos.2019.105179

Wilson, I. H. (1978). Volcanism on a Proterozoic continental margin in northwestern Queensland. *Precambrian Research*, *7*(3), 205–235. https://doi.org/10.1016/0301-9268(78)90039-6

Wilson, I. H. (1983). Geochemical discrimination of acid volcanic units in the Mount Isa region, Queensland. *BMR Journal of Australian Geology & Geophysics*, *8*(2), 109–117.

Wilson, I. H. (1987). Geochemistry of Proterozoic Volcanics, Mount Isa Inlier, Australia. *Geological Society, London, Special Publications*, *33*, 409–423. https://doi.org/10.1144/GSL.SP.1987.033.01.28

Withnall, I. W. (2019). *Review of SHRIMP zircon ages for the Eastern Succession of the Mount Isa Province and magmatic events in its provenance*. Department of Natural Resources, Mines and Energy.

Withnall, I. W., & Hutton, L. J. (2013). North Australian Craton. In P. A. Jell (Ed.), *Geology of Queensland* (pp. 23–112). Geological Survey of Queensland.

Wyborn, L. A. I. (1988). Petrology, geochemistry and origin of a major Australian 1880-1840 Ma felsic volcano-plutonic suite: A model for intracontinental felsic magma generation. *Precambrian Research*, *40–41*, 37–60. https://doi.org/10.1016/0301-9268(88)90060-5

Wyborn, L. A. I., Bastrakova, I. V., Hensley, C., & Budd, A. R. (2001). Mount Isa Inlier. In A. R. Budd, L. A. I. Wyborn, & I. V. Basyrakova (Eds.), *The metallogenic potential of Australian Proterozoic Granites* (pp. 92–96). Geoscience Australia.

Wyborn, L. A. I., & Page, R. W. (1983). The Proterozoic Kalkadoon and Ewen Batholiths, Mount Isa Inlier, Queensland: Source, chemistry, age, and metamorphism. *BMR Journal of Australian Geology & Geophysics*, *8*(1), 53–69.

Wyborn, L. A. I., Page, R. W., & McCulloch, M. T. (1988). Petrology, geochronology and isotope geochemistry of the post-1820 Ma granites of the Mount Isa Inlier: Mechanisms for the generation of Proterozoic anorogenic granites. *Precambrian Research*, *40–41*, 509–541. https://doi.org/10.1016/0301-9268(88)90083-6

Wyborn, L. A. I., Wyborn, D., Warren, R. G., & Drummond, B. J. (1992). Proterozoic granite types in Australia: Implications for lower crust composition, structure and evolution. *Earth and Environmental Science Transactions of the Royal Society of Edinburgh*, *83*(1–2), 201–209. https://doi.org/10.1017/S0263593300007896

Zhao, G., Sun, M., Wilde, S. A., & Li, S. (2004). A Paleo-Mesoproterozoic supercontinent: Assembly, growth and breakup. *Earth-Science Reviews*, *67*(1–2), 91–123. https://doi.org/10.1016/j.earscirev.2004.02.003

Zhao, J. X., & Bennett, V. C. (1995). SHRIMP U-Pb zircon geochronology of granites in the Arunta Inlier, central Australia: Implications for Proterozoic crustal evolution. *Precambrian Research*, *71*(1-4), 17–43. https://doi.org/10.1016/0301-9268(94)00054-U

Zhao, J. X., & McCulloch, M. T. (1995). Geochemical and Nd isotopic systematics of granites from the Arunta Inlier, central Australia: Implications for Proterozoic crustal evolution. *Precambrian Research*, *71*(1–4), 265–299. https://doi.org/10.1016/0301-9268(94)00065-Y